sCO2-4-NPP: Innovative sCO2-Based Heat Removal Technology for an Increased Level of Safety of Nuclear Power Plants

Deliverable 4.3

Conceptual design of the sCO2-4-NPP turbomachine

Work programme topic addressed: NFRP-2018-10: Encouraging innovation in nuclear safety for the benefit of European citizen

Type of action: Innovation action

Grant Agreement number:	847606
Start date of project: 1 September 2019	Duration: 36 months
Lead beneficiary of this deliverable:	UDE
Due date of deliverable: 31/08/2022	Actual submission date: 31/08/2022
	Version #: R1.0

Type		
R	Document, report excluding the periodic and final reports	X
DEM	Demonstrator, pilot, prototype, plan designs	
DEC	Websites, patents filing, press & media actions, videos, etc.	
OTHER	Software, technical diagram, etc.	
Dissemination level		
PU	PUBLIC, fully open, e.g. web	X
CO	CONFIDENTIAL, restricted under conditions set out in Model Grant Agreement	

This project has received funding from the Euratom research and training programme 2014-2018 under grant agreement No 847606. This document and its contents remain the property of the beneficiaries of the sCO2-4-NPP Consortium and may not be distributed or reproduced without the express written approval of the Coordinator, EDF.

Revision History

Release	Date	Reason for Change	Author	Distribution
R0.1	15.07.2022	First draft	Haikun Ren	Sebastian Schuster Dieter Brillert
R0.2	01.08.2022	Internal review	Haikun Ren	Albannie Cagnac Jörg Starflinger Susan Barreault
R0.3	19.08.2022	Internal review	Haikun Ren	All partners
R1.0	31.08.2022	Final version	Haikun Ren	Public

Deliverable Contributors

Authors

Partner	Name
UDE	Haikun Ren

Contributors

Partner	Name
UDE	Haikun Ren
UDE	Alexander Hacks

Internal Reviewers

Partner	Name
UDE	Sebastian Schuster
UDE	Dieter Brillert
EDF	Albannie Cagnac
USTUTT	Jörg Starflinger

Table of contents

List of Figures

1 List of Acronyms

Abbreviation / Acronym	Description / meaning
A	Alternator
AMB	Active Magnetic Bearing
ATHLET	Analysis of Thermal-hydraulics of Leaks and Transients
C	Compressor
CAD	Computational Aided Design
CATHARE	Code for Analysis of THermalhydraulics during an Accident of Reactor and safety Evaluation
CHX	Compact Heat eXchanger
CVR	Centrum Vyzkumu Řež S.R.O.
D	Deliverable
DUHS	Diverse Ultimate Heat Sink
GfS	GfS Gesellschaft für Simulatorschulung mbH
NPP	Nuclear Power Plant
NP TEC	Nuovo Pignone Tecnologie SRL
P&ID	Piping and Instrumentation Diagram
sCO_2	Carbon dioxide in supercritical state
sCO2-HeRo^B	sCO2-HeRo turbomachine with ball bearings
sCO2-HeRo^M	Improved sCO2-HeRo turbomachine with magnetic bearings
T	Turbine
TAC	Turbo-Alternator-Compressor
TRL	Technical Readiness Level
UDE	University of Duisburg-Essen
USTUTT	University of Stuttgart
WP	Work Package
2D	Two Dimensional
3D	Three Dimensional

2 Executive Summary

The project sCO2-4-NPP intends to improve the safety level of European nuclear power plants (NPPs) by developing a heat removal system as a backup cooling system. This system consists of several identical modules based on the Joule-cycle using carbon dioxide at supercritical state (sCO_2) as its working fluid. Due to the modular design, it is possible to retrofit the system in existing European NPPs as well as the next generation. Furthermore, each module should be self-launching and self-propelling, so that human intervention can be significantly reduced. The turbomachine is an essential part of the whole heat removal system. The sCO2-4-NPP turbomachine has been designed to fulfil the objectives of the project, and results are reported in this deliverable.

Generally, the design of the sCO2-4-NPP turbomachine is based on the concept of the turbomachine sCO2-HeRo^B, whose size is smaller than the sCO2-4-NPP turbomachine. The superscript “B” means that ball bearings have been applied for this turbomachine. This smaller machine has been validated in “laboratory environment (TRL3)” in the previous EU funded project sCO2-HeRo and has been further improved in this project, resulting in the turbomachine called sCO2-HeRo^M, in which active magnetic bearings (denoted by superscript “M”) are employed instead of ball bearings to improve the robustness of the turbomachine. The turbomachine is a turbo-alternator-compressor (TAC), where the turbine, alternator, and compressor are on one shaft. Such a design allows a compact structure and enables self-launching and self-propelling properties.

The TAC, as a component of the whole cycle, is influenced by the other cycle components. In turn, it affects them as well. Therefore, the design of the TAC and the cycle as a whole is conducted in parallel. UDE provides the performance maps of the TAC, which are incorporated into the cycle simulation codes (ATHLET, CATHARE and Modelica). In turn, the cycle simulation results indicate that the design fulfils the thermodynamic requirement of the cycle. This work contributes to further developing this heat removal technology to TRL5, namely validation of components in a simulated environment.

The mechanical components of the TAC are scaled-up from those of sCO2-HeRo^M, since the experiments with regard to sCO2-HeRo^M already verified their robustness. The scale-up factors relate to fundamental functional parameters like force, power or pressure and lead to reliable conclusions. The design also includes the main dimensions and mechanical interfaces of the sCO2-4-NPP TAC. They contribute to the architectural design of the entire sCO_2 module and give a first impression of what a sCO_2-TAC would look like on a 1:1 scale.

Furthermore, required additional systems are also considered. These include the additional cooling system for magnetic bearings and alternator and a piston pump to start the module from a cold standstill, which are designed in this project and verified with sCO2-HeRo^M. Their description contributes to a better understanding of the operation strategy regarding the sCO_2 loop around the TAC and exhibits practical information to cycle designers.

3 Introduction

To increase the safety level of nuclear power plants (NPPs) in case of accidents, a concept of a sCO_2-based heat removal system has been formulated by Venker [1]. This concept has been validated at laboratory conditions (TRL3) in the sCO2-HeRo project. Based on the results and knowledge gained from the sCO2-HeRo project, the system is scaled up in the sCO2-4-NPP project based on real NPP dimensions to bring this technology closer to market (whole system to TRL5 and part of the system to TRL6).

The basic requirement of the heat removal system is to remove the decay heat from the reactor core after an accident, where the decay heat is declining over time. Figure 1 shows an example of the declining decay heat $\dot{Q}_{decay}$ denoted by the blue curve. The cooling power of the heat removal system, namely the heat input $\dot{Q}_{in}$ into the heat removal system, needs to adapt to the decay heat. This requires that the system's cooling power achieves its maximum right after the start-up and then reduces continuously afterwards. The orange curve shown in Figure 1 illustrates the cooling power of the system, which consists of four modules. This concept allows the shutdown of one module after another to increase the heat input to each remaining module. Further, it reduces the requirement on the operation range regarding the heat input of a single module.

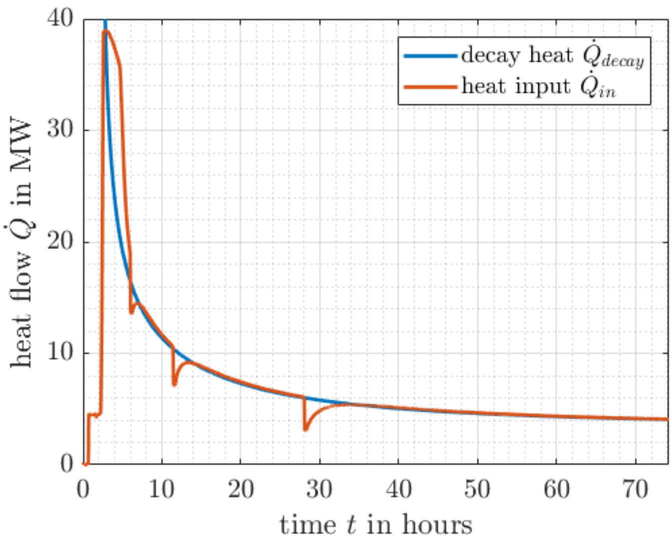

Figure 1: Decay heat of the reactor core and heat input to the heat removal system (removed heat) over time

Each module of the system is powered by an integrated Joule-cycle using carbon dioxide over the so-called critical states ($p_{crit} = 73.7$ bar and $T_{crit} = 31$ °C) as its working fluid. These modules can be self-starting and self-propelling without external power sources, delaying the need for human intervention and therefore decreasing the risk of human errors, when an accident in a NPP occurs. Figure 2 illustrates the concept of the module (i) of the system, in which the TAC is marked by the dashed box. The sCO_2 flow is first pressurised by the compressor (C) and heated via the compact heat exchanger (CHX) by transmitting the heat $\dot{Q}_{in,i}$ from the secondary loop of the NPP. Thereafter, the flow is expanded by the turbine and then cooled by the diverse ultimate heat sink (DUHS). During this process, the expansion work produced by the turbine simultaneously drives the alternator and compressor. This requires that the turbine's power must be higher than that expended by the alternator and the compressor. The surplus power, or exceed power, is converted into electrical power $P_{el,i}$ by the alternator and can be utilised for other applications, e.g., controlling the rotational speed of the rotor.

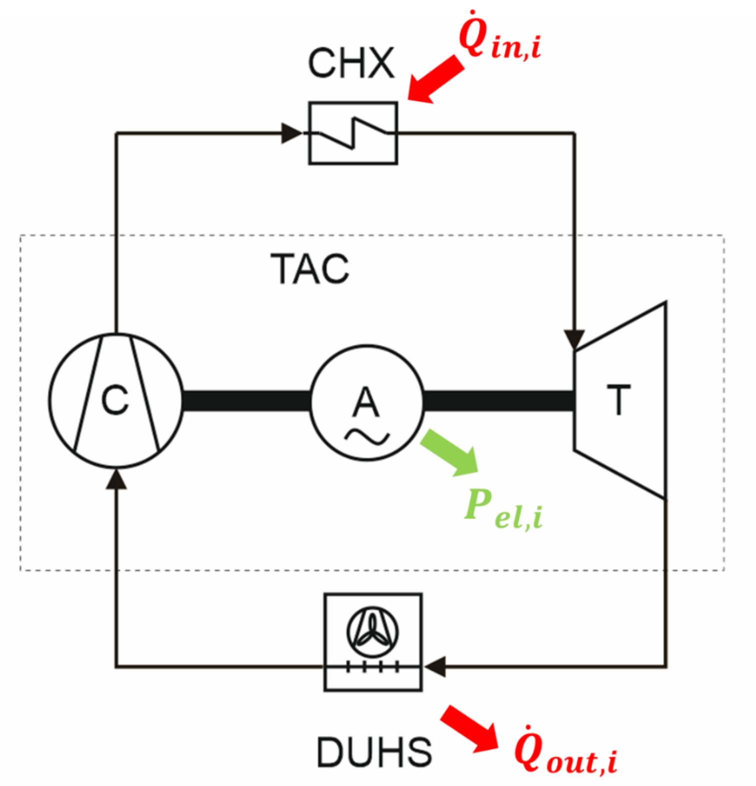

Figure 2: Concept of the module and the turbomachine

The aerodynamic design of the sCO2-4-NPP TAC is conducted through an iterative process in close cooperation with the cycle design. The reason is that the design parameters of both TAC and cycle influence each other. The design parameters are obtained by applying the design tool [2] developed by UDE in the sCO2-Flex project. Thereafter, the performance maps of the TAC are generated by using off-design tools [3] [4] developed by UDE and provided as turbomachine models for the simulations to be implemented in thermodynamic simulation code like ATHLET, CATHARE and Modelica. The verification of the design is achieved by identifying the operating line of the TAC extracted from the simulation results within the performance maps and by comparing the total heat input of the system with the decay heat, as shown in Figure 1.

The mechanical design of the TAC is strongly affected by the experience gained in the sCO2-HeRo project. The initial tests conducted in the SUSEN CO_2-loop at CVR Research Center Řež [5] have validated the feasibility of such a TAC design (sCO2-HeRo^B with "B"all bearings). The following tests conducted in GfS in Essen exhibit the reproducibility of the experiment and verify the robustness of the improvement of the TAC design (sCO2-HeRo^M with active "M"agnetic bearings), for example, applying the magnetic bearing technology to solve the issues of classic ball bearings. This brings the sCO_2 heat removal system to a higher technology readiness level and provides knowledge and experience for the TAC design in the sCO2-4-NPP project. Therefore, the mechanical components of the sCO2-4-NPP TAC are designed following their design concepts applied in sCO2-HeRo^M. For example, the magnetic bearings are obtained based on the initial design in sCO2-HeRo^M by considering a scaling-up factor, which is calculated by estimating the bearing force of both designs. With this factor, the significant geometry like pole surface of the scaled-up design is derived. Finally, the design process is exhibited in Figure 3.

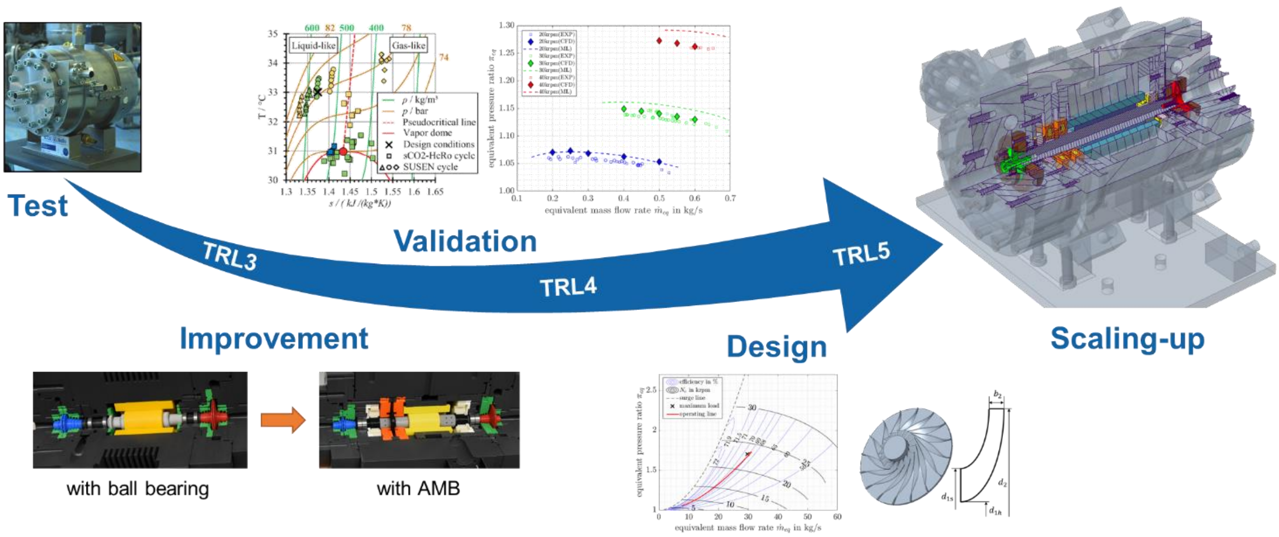

Figure 3: Design process of sCO2-4-NPP turbomachine

In summary, this report presents the final conceptual design of the sCO2-4-NPP TAC, including important information for other work packages in the sCO2-4-NPP project. In chapter 4, the aerodynamic design and off-design are introduced. In chapter 5, the mechanical design, including bearings, seals, shaft and casing, is exhibited. In chapter 6, the defined auxiliaries of the TAC are described. Finally, conclusions and outlooks are addressed in chapter 7.

4 Aerodynamic design

4.1 Compressor design

4.1.1 Design concept

In most energy conversion cycles, a single design point of the system can be specified, at which the system operates most efficiently. In contrast, the sCO2-4-NPP system and its modules are not operated at a single point, but along with the declining decay heat, see Figure 1. Therefore, instead of finding an optimum compressor for a single operating point, the sCO2-4-NPP compressor is designed for a wide operation range. To achieve this goal, an initial design is obtained with an educated guess for the cycle parameters followed by an iterative modification of mass flow rate and compressor pressure ratio until a sufficient design is achieved.

The aerodynamic design of the compressor employs a design tool for sCO_2 centrifugal compressors based on the two-zone model [2], which UDE developed in the Horizon 2020 project sCO2-Flex. By specifying the required design parameters, the design tool calculates the flow properties at certain sections in the compressor and determines the main dimensions of the compressor, including the impeller and the diffuser with the help of the Cordier-diagram [6]. The design of the volute follows the concept mentioned by Bohl [7].

4.1.2 Performance including simulation results

To guarantee a quick and a reliable prediction of the compressor performance, an off-design tool based on mean-line analysis incorporating appropriate loss coefficients [3] is developed by UDE in this project. The off-design tool is built and running within MATLAB. Based on the mass flow rate, the rotational speed, the thermodynamic conditions like pressure and temperature at the inlet, and the main geometry of the compressor, the flow properties at certain sections such as impeller inlet, impeller outlet, diffuser outlet, volute outlet and exit cone outlet are calculated. Thereafter, the performance of the compressor, like pressure ratio and efficiency vs. mass flow rate, can be illustrated. This tool is validated with the CFD results of the sCO2-HeRo compressor. The validation is already mentioned in the deliverable D4.2 and [3].

Figure 4 shows the performance of the compressor regarding the pressure ratio vs. the mass flow rate. The isolines of the rotational speed and the efficiency[1] are denoted by black and blue contour respectively. The dashed line denotes the states, where surging occurs, and, therefore, should be avoided. Furthermore, the figure also shows the operating line of the compressor extracted from the simulation results of the last module from ATHLET. Since all the active modules have the same performance at the same time, the last module exhibits the most extensive range of the operation performance. It is denoted by the thick red curve and starts at the maximum load of the module, namely the thermodynamic design point of the cycle. The values of the operating line are corrected[2] by referencing the nominal thermodynamic condition of the compressor inlet. It can be observed that the operation starts at position X. Subsequently, the operating point moves towards the original point along the isolines of the efficiency by reducing the rotational speed and the mass flow rate simultaneously. The operating line is far away from the surge line, or in other words, with a relatively large surge margin, which means a safe operation. Besides, the operating line is located near the 70 % isoline. This

[1] Considering additional power loss on the shaft, the efficiency of the compressor is corrected by multiplying a factor of 7/8.

[2] The correction method is attached in Appendix A.1.

indicates a relatively efficient operation of the compressor since there is no efficiency loss during the operation. Consequently, the compressor design fulfils the thermodynamic requirement of the cycle module.

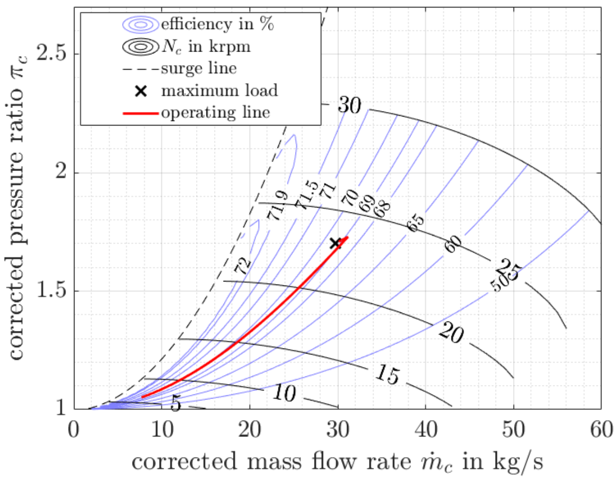

Figure 4: Performance map of the sCO2-4-NPP compressor regarding pressure ratio vs. mass flow rate including the operating line

4.1.3 Main dimensions

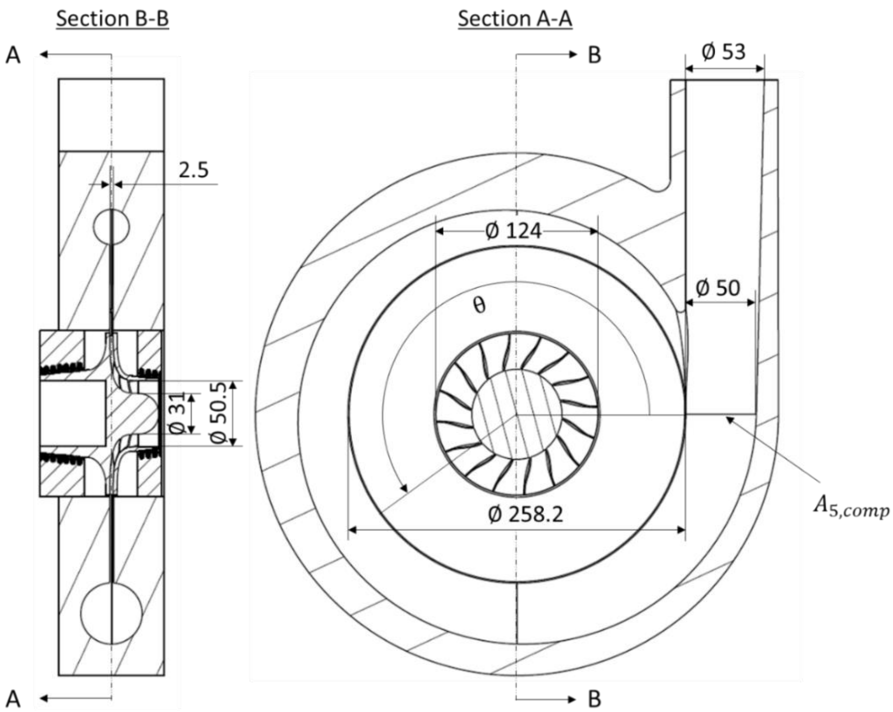

Figure 5: Main dimensions of the sCO2-4-NPP compressor (unit in mm)

Figure 5 illustrates the main dimensions of the sCO2-4-NPP compressor. The compressor has a 3D shrouded impeller and a vaneless diffuser. The height of the diffuser is constant and equal to the blade height at the impeller outlet. The dimensions are obtained from the design tool mentioned above except the dimensions of the volute. The diameter of the compressor outlet (exit cone outlet) is calculated by [7] as

$$d_{out,comp} = \sqrt{\frac{\dot{V}_{out,comp}}{k_a \cdot \sqrt{2 \cdot \Delta h_{is,comp}}} \cdot \frac{4}{\pi}} \quad , \tag{1}$$

where $\dot{V}_{out,comp}$ is the volume flow rate at the compressor outlet, $\Delta h_{is,comp}$ is the specific isentropic enthalpy rise through the compressor and k_a is an empirical factor equal to 0.1. The area of the volute outlet ($A_{5,comp}$) is then defined as 90 % of that of the compressor outlet. The volute casing has a circular cross-section, whose area is calculated by [7] as

$$A_\theta = \frac{\theta}{360°} \cdot A_{5,comp} \quad , \tag{2}$$

where the angle θ is given in degrees. Information on the blades is given in Appendix B.1.

4.2 Turbine design

4.2.1 Design concept

The turbine design in sCO2-4-NPP is closely related to the sCO2-HeRo turbine. The ratio of the pressures across the turbine is a little lower than that of the compressor at the nominal condition because of the pressure drops in the compact heat exchanger and pipes. The design parameters are obtained by a design tool based on mean-line analysis, in which the calculation of the dimensions follows the centripetal turbine design by Bohl [7].

4.2.2 Performance including simulation results

Similar to the compressor off-design, an off-design tool for the turbine has been developed by UDE in this project based on mean-line analysis by employing the enthalpy loss coefficients mentioned by Schuster et al. [4]. This tool also defines several sections to calculate the flow properties. Based on the inlet conditions and the main geometry of the turbine, the tool outputs the turbine's performance maps. The tool is validated with the CFD simulation results of the sCO2-HeRo TACs mentioned in the last deliverable D4.2.

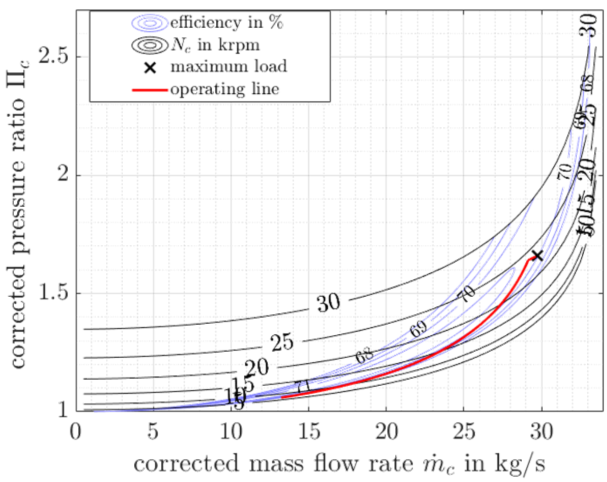

Figure 6: Performance map of the sCO2-4-NPP turbine regarding pressure ratio vs mass flow rate including the operating line

Figure 6 shows the performance map of the turbine, including the contour of the rotational speed (black) and the efficiency[3] (blue). The simulation within ATHLET results in the operating line denoted by the red thick curve starting from the so-called maximum load of the module (X). Similar to the compressor, the values are corrected relating to the reference condition at the turbine inlet (thermodynamic design point of the cycle). The course of the red curve exhibits an efficiency of around 70 % within the operation range of the turbine. This points out that the operation of the turbine is also efficient. Note that the corrected mass flow rate of the turbine is different to that of the compressor due to the different change of the inlet conditions of both components.

4.2.3 Main dimensions

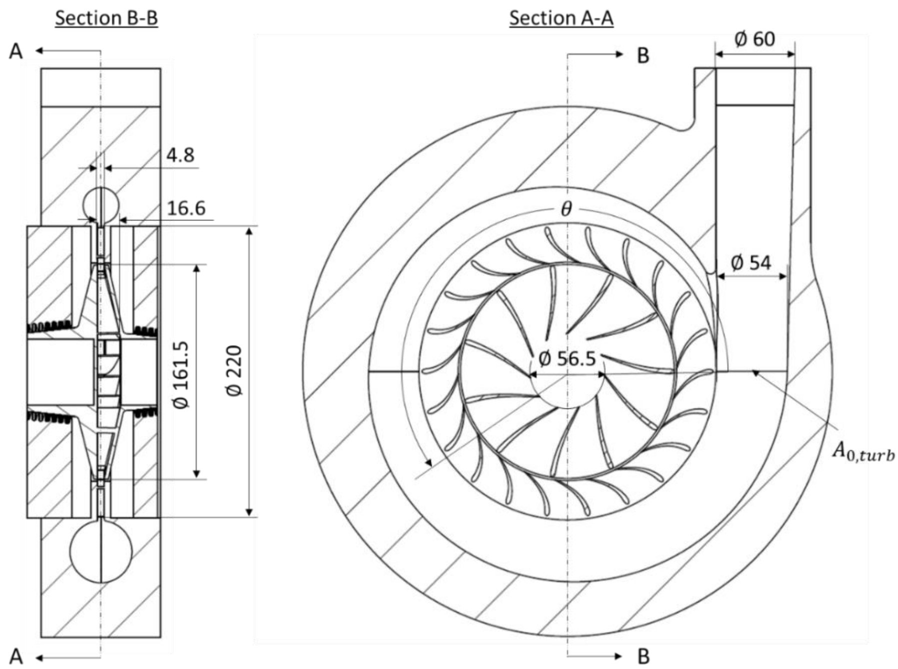

Figure 7: Main dimensions of the sCO2-4-NPP turbine (unit in mm)

Figure 7 illustrates the main dimensions of the sCO2-4-NPP turbine. The turbine has a 2D shrouded impeller. The height of the nozzle is constant and equal to the blade height at the impeller inlet. Similar to the compressor's design, the diameter of the turbine inlet is calculated by [7]

$$d_{in,turb} = \sqrt{\frac{\dot{V}_{in,turb}}{k_e \cdot \sqrt{2 \cdot \Delta h_{is,turb}}} \cdot \frac{4}{\pi}}, \quad (3)$$

where $\dot{V}_{in,turb}$ is the volume flow rate at the turbine outlet, $\Delta h_{is,turb}$ is the specific isentropic enthalpy drop of the turbine and k_e is an empirical factor equal to 0.16. The area of the volute inlet ($A_{0,turb}$) is 80 % of the area of the turbine inlet. The volute of the turbine also has a circular cross-section and the area is calculated by eq. (2), where $A_{5,comp}$ needs to be replaced by $A_{0,turb}$. Information on the blades is given in Appendix B.2.

[3] The efficiency of the turbine is also multiplied by a factor of 7/8 by considering the additional power need as same as that of the compressor.

4.3 Turbomachine performance

In this section, the performance of the turbomachine's net power with respect to the simulation results is presented by considering the windage loss and the power loss due to leakage. Due to numerical issues, it is a challenge to incorporate these losses into the simulation codes. Therefore, they are calculated separately. In the first part of this section, the losses are described and the calculation results are shown. In the second part, the net power of the TAC is shown.

4.3.1 Consideration of losses

4.3.1.1 Windage loss

One of the main losses normally considered inside the TAC is the windage loss, which is caused by the friction force due to the relative movement between the fluid and the surface of the components. Windage loss can be found at the disk of the compressor and the turbine, and at the rotor of the alternator. Since the windage loss of the disks is already considered with the conservative estimation of the efficiency of both the compressor and the turbine, the remaining windage loss, which should be considered here, is the friction loss due to rotation of the alternator rotor.

The calculation of the windage loss is based on the model by Bilgen and Boulos [8] and written as

$$P_{loss,alternator} = \frac{1}{2} \cdot C_m \cdot \rho \cdot \omega^3 \cdot r^4 \cdot l, \tag{4}$$

where ρ is the density of the fluid, ω is the angular velocity, r is the rotor radius, l is the rotor length and C_m is the torque coefficient calculated by

$$C_m = \frac{0.065 \cdot \left(\frac{b}{r}\right)^{0.1}}{Re^{0.2}}, \tag{5}$$

in which b represents the gap width between the alternator rotor and stator, and Re the Reynolds number[4].

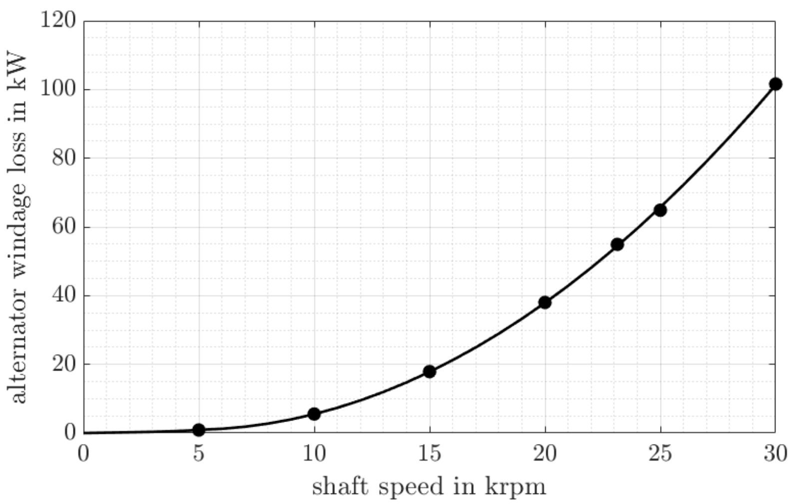

Figure 8: Windage loss of the alternator vs rotational speed at the reference conditions

[4] Bilgen and Boulos [8] define $Re = \frac{\rho \omega r b}{\mu}$.

The calculation results are displayed in Figure 8, in which the windage loss of the alternator is given over the rotational speed at the nominal condition. It shows a quasi-parabolic curve and a windage loss of 55 kW at the designed rotational speed (23 krpm). This kind of loss is to be considered in the further calculation and estimation of the TAC's power characteristics.

4.3.1.2 Power loss due to leakage and additional cooling

Another main loss detected in the TAC is the so-called leakage loss, which is caused by the leakage flow through the labyrinth seals and some other flow paths. Especially for the sCO2-4-NPP TAC, there is an additional cooling system designed for cooling the magnetic bearing and the alternator, which will extract the cold sCO_2 flow from the loop and lead it into the TAC. Due to the requirement of a pressure difference, the extraction point is located between the compressor's outlet and the CHX's inlet. This configuration causes a double leakage (from the compressor shaft seal and the extraction point) between the compressor's inlet and the turbine's inlet. Hence, the turbine is never operated with the same mass flow rate as the compressor. This reduces pressure ratio via the turbine. As shown by the example in Figure 9, this reduction (from $\dot{m}_3$ to $\dot{m}_3'$) causes an imbalance of the pressure ratios between the compressor and the turbine, which should be overcome by increasing the mass flow rate at the compressor's inlet (from $\dot{m}_1$ to $\dot{m}_1''$) while the leakage is kept constant. The pressure ratio of the compressor and the turbine is different since the pressure losses in the CHX, DUHS and the pipes are considered.

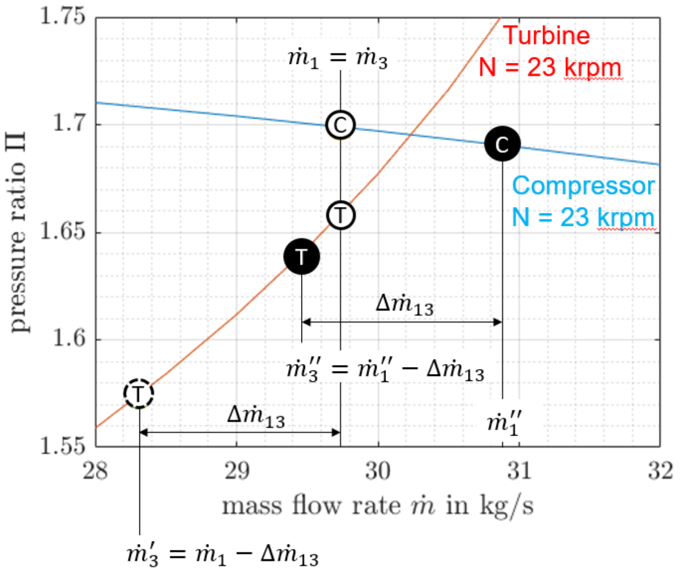

Figure 9: Balancing of the compressor and turbine's pressure ratio

Such variation of the mass flow rate also changes the compressor and the turbine's power. Figure 10 illustrates the reduction of power produced by the turbine and the increase of the power needed by the compressor corresponding to the change of the pressure ratios in Figure 9. It means that by considering a leakage of about 1.4 kg/s between the compressor and turbine's inlet, the net power[5] produced by the whole TAC decreases from P to P''. In this example, the power loss ratio defined by

[5] The net power of the TAC is defined here as the difference between the power produced by the turbine and the power required by the compressor.

$$\frac{\Delta P_{loss}}{P} = \frac{P - P''}{P} \times 100\%, \tag{6}$$

is about 11.8 %, where P and P'' are the net power without and with considering the leakage.

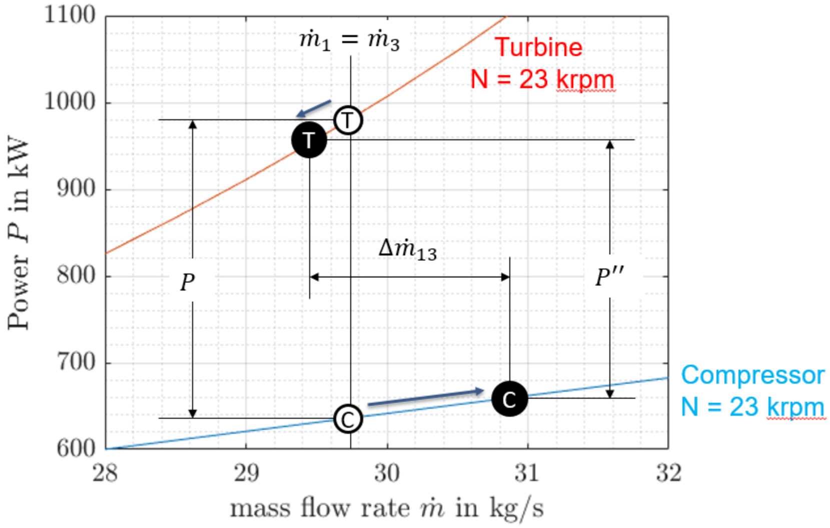

Figure 10: Impact of the leakage on power performance of the TAC

According to the statement above, the power loss of the TAC due to the leakage depends on the leakage mass flow rate or the leakage ratio, which can be defined as

$$lr = \frac{\Delta\dot{m}_{lk}}{\dot{m}_1} = \frac{\dot{m}_1 - \dot{m}_3}{\dot{m}_1} \times 100\%. \tag{7}$$

Based on the structure of the sCO_2 cooling system and the simulation results from ATHLET, the leakage ratio and the power loss ratio can be calculated by modelling the additional cooling[6] and estimating the leakage through the shaft seal of the compressor and the turbine, and the extraction point. Consequently, a conservative estimation regarding the leakage ratio and the power loss ratio is conducted and the results are shown below. Figure 11 (left) exhibits the correlation between the leakage ratio and the power loss ratio, while Figure 11 (right) displays curves of both regarding the simulation time. In the first 4.5 hours, the power loss ratio decreases against the increasing leakage ratio, because the thermodynamic inlet condition of the turbine is not stable and changing dramatically. Thereafter, both power loss and leakage ratio reduce due to the reduced mass flow rate and rotational speed. In summary, the power loss ratio is generally getting lower, as the leakage ratio becomes less. Although the power loss ratio reached a maximum value of 14 %, in the most operation time the power loss is lower than 7 %. Since the estimation is relatively conservative, the loss could be lower than expected.

[6] The modeling of the additional cooling is based on the cooling concept from Task 4.1 in this project and its description are given in Appendix A.2.

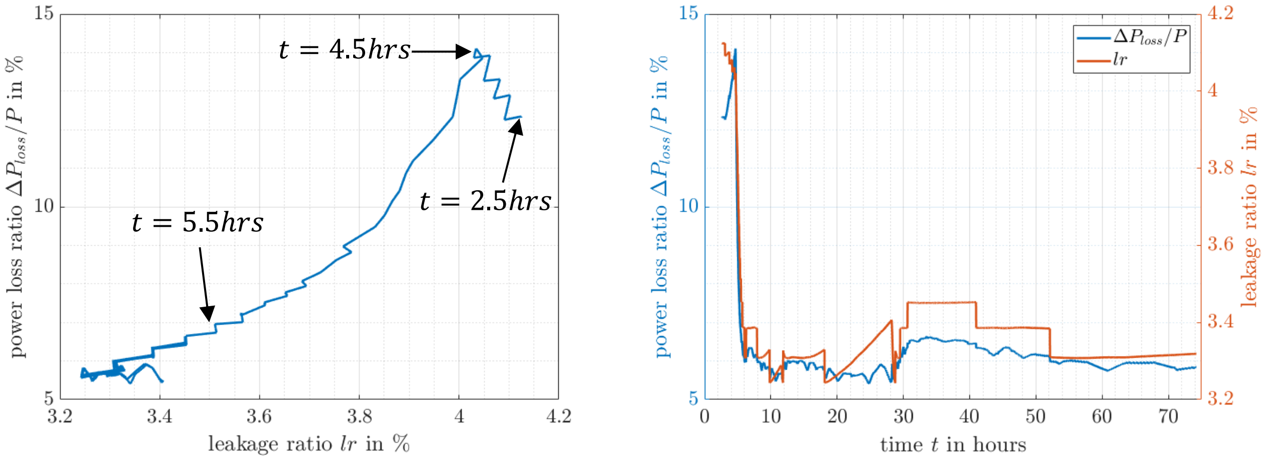

Figure 11: Estimation of the power loss ratio and the leakage ratio based on the simulation results

4.3.2 Excess power

Considered the losses mentioned above, the net power of the TAC is reduced further. However, positive net power is required. Therefore, a calculation is implemented to check whether this requirement is fulfilled. The calculation of the final net power is expressed by

$$P'' = P - P \cdot \frac{\Delta P_{loss}}{P} - P_{loss,alternator} - P_{fan}, \tag{8}$$

in which the term P_{fan} represents the power need of the cooling fans mounted in the module. The value of the fan power is given by the simulation results.

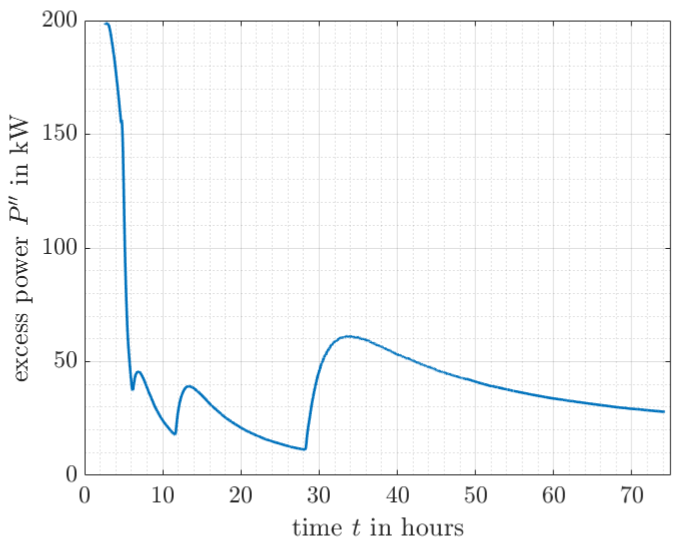

Figure 12: Net power of the sCO2-4-NPP TAC corresponding to the simulation

Finally, the net power of the TAC based on the simulated operation is shown in Figure 12. Obviously, it indicates an operation with excess power of the TAC during the 72 hours simulation. It shows the maximum net power of 200 kW at the beginning, where the module is at its maximum load. It also exhibits the minimum net power at about 29 hours, whose value is already over 10 kW. The result indicates not only a sufficient net power (exceed power) at the module's maximum load, but also positive net power during the whole operation by considering the main losses in the module conservatively. Besides, the net power of the TAC remains 30 kW at the end of the simulation and indicates that the last module can still remove the decay heat for a longer time. Since the task of the sCO2-4-NPP system or modules is mainly to remove the decay heat not to generate power, the design has already fulfilled the requirement according to the results, and even a benefit of excess power can be expected.

5 Mechanical design

5.1 Bearings

To solve the issues of ball bearings such as oil dissolution in sCO_2 detected in the previous project, active magnetic bearing (AMB) technology is applied for improving the TAC design. This technology has been verified by the tests conducted with sCO2-HeRo^M in Essen in this project, and hence, is recommended for the scaled-up TAC machine. There are two radial AMBs and one axial AMB. The radial AMBs are applied as floating bearings at the compressor side and turbine side of the rotor respectively, while the axial AMB is mounted as thrust bearing at the compressor side. Safety bearings, also called touchdown bearings, are employed at both sides of the rotor. They can mitigate the damage on the machine in case of overloads or magnetic bearing's failure.

5.1.1 Radial bearing

The scaling-up of the radial AMB is based on the design concept of radial AMBs mentioned in [9] [10], where the relationship between the pole surface area A_{gr} and the maximum force F_{max} is written as

$$A_{gr} = \frac{F_{max} \cdot \mu_0}{B_{max}^2 \cdot \epsilon \cdot \cos(\alpha)} = w_p \cdot L, \quad (9)$$

in which the maximum magnetic flux density, the vacuum permeability, the fringing and leakage reduction factor, the pole angle, the pole width, and the axial length are denoted by B_{max}, μ_0, ϵ, α, w_p and L respectively. By assuming that the radial and axial AMBs applied in both TACs have the same value of ϵ and α, as well as B_{max} and μ_0, the pole surface area is proportional to the maximum force, namely $A_{gr} \propto F_{max}$. To calculate the maximum radial bearing force, UDE establishes a calculation tool, which is used for designing the radial AMBs of sCO2-HeRo^M. The test results of sCO2-HeRo^M show that the machine with the designed radial AMBs works well. This indicates that the bearing force calculated by this tool is never underestimated. Thus, this calculation tool is regarded as valid for the preliminary design of radial AMBs and applied here. Finally, the maximum radial force on the sCO2-HeRo^M rotor is 150 N and on the sCO2-4-NPP rotor is 400 N. This results in a 2.7 times larger pole surface area of the sCO2-4-NPP radial AMB.

Figure 13 illustrates the main dimensions of a radial AMB. Generally, h represents the height, r the radius, while subscript p relates to the poles and c to the coils. f_s and w_p are the thickness coefficient of ironclad magnet and the pole width respectively. By specifying several parameters like the inner diameter r_r, the journal ratio γ, and the pole surface area A_{gr}, other parameters can be initially calculated by [10] as

$$w_p = \frac{-\gamma r_r + \sqrt{2\gamma A_{gr} f_s + \gamma^2 r_r^2}}{2\gamma f_s}, \quad (10)$$

$$r_j = r_r + f_s \cdot w_p, \quad (11)$$

$$r_{si} = r_p + h_p, \quad (12)$$

$$r_{so} = r_{si} + f_s \cdot w_p. \quad (13)$$

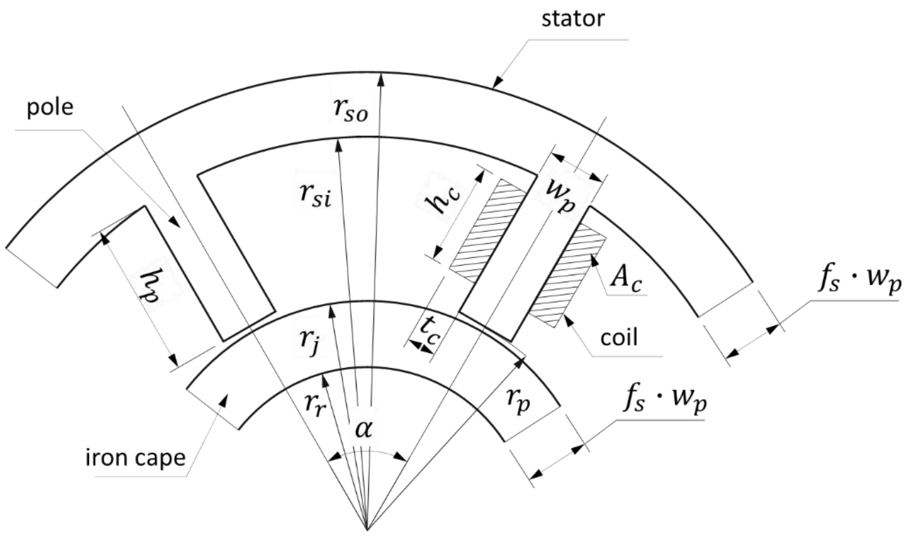

Figure 13: Coaxial cross-section of a radial AMB [10]

The coil thickness t_c, the coil height h_c and the pole height h_p are determined to guarantee sufficient magnetic flux and bearing force. The axial length is then calculated by applying eq. (9). To ensure a robust design, recommendations from "MECOS AG", who is the magnetic bearing manufacturer for sCO2-HeRo^{M}, are considered. Finally, the scaled-up radial AMB is shown below, in contrast with the original one.

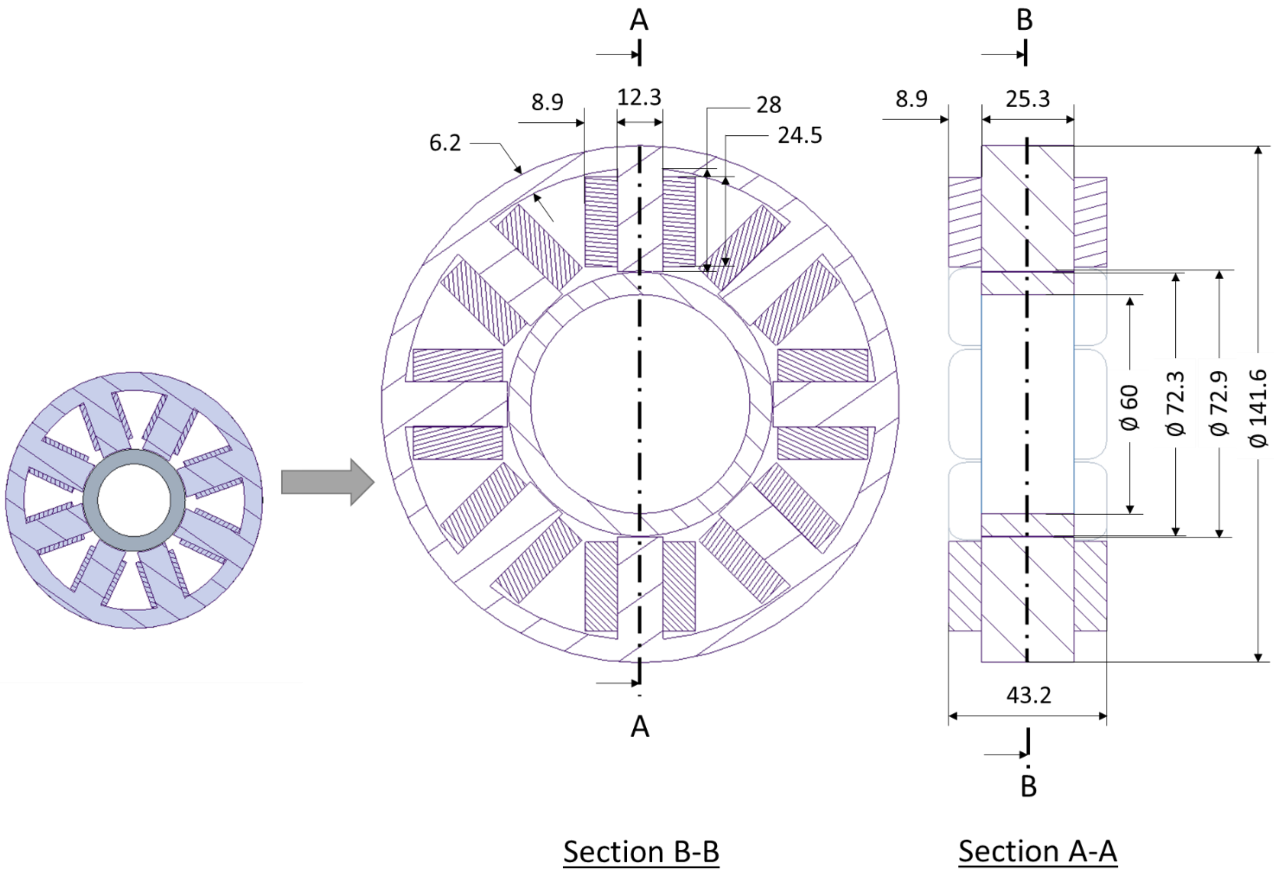

Figure 14: Scaling-up of radial AMB from sCO2-HeRo^{M} to sCO2-4-NPP size (unit in mm)

5.1.2 Axial bearing

Similar with the scaling-up concept of the radial AMB, the design concept of the axial AMB from [11] is considered. It also describes a proportional correlation between the thrust F and the pole surface area A_{ga}

$$F = \frac{B_{max}^2}{\mu_0} \cdot A_{ga}, \tag{14}$$

if B_{max} and μ_0 remain constant. A typical axial AMB's geometry can be illustrated by the figure shown below.

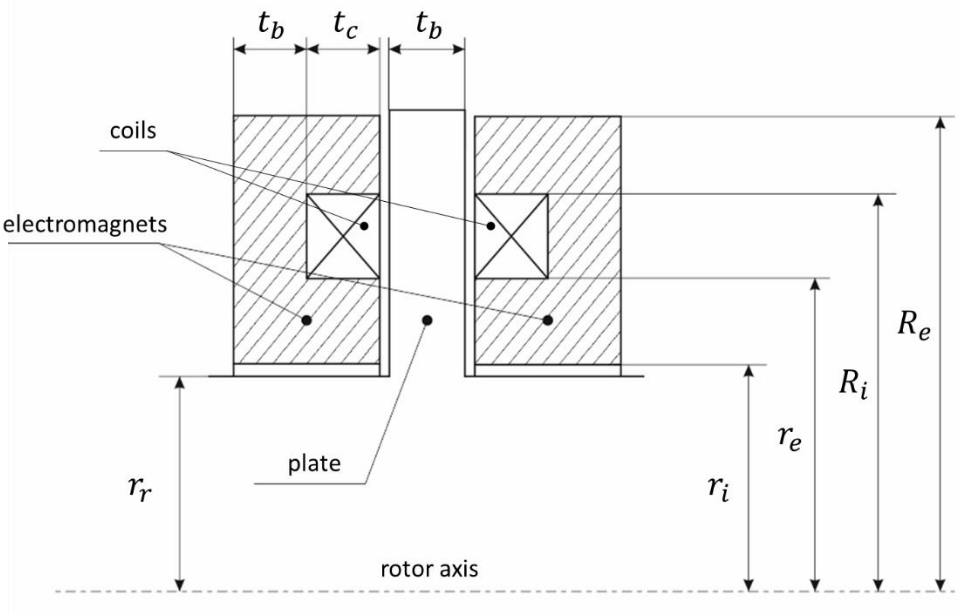

Figure 15: Cross-section of axial AMB [11]

According to Figure 15, the pole surface area is expressed by

$$A_{ga} = \pi\left(r_e^2 - r_i^2\right) = 2\pi r_e t_b = \pi\left(R_e^2 - R_i^2\right) = \frac{F_{thrust} \cdot \mu_0}{B_{max}^2}, \tag{15}$$

where r_i, r_e, t_b, t_c, R_i and R_e represent the inner radius of the inner pole, the external radius of the inner pole, the thickness of the thrust plate, the thickness of the coil, the inner radius of the external pole and the external radius of the external pole.

The calculation of the thrust on the axial AMB is conducted via a calculation tool developed by UDE within this project, in which the forces working on the main axial surfaces of the rotor due to the static pressure are calculated. These forces result in a thrust, which is finally to be balanced. This tool is also verified via the experiments in terms of sCO2-HeRo[M] conducted in Essen. The calculation results show a thrust of 250 N on the sCO2-HeRo rotor, while it is about 3000 N in sCO2-4-NPP. This means that the axial AMB's pole surface in the sCO2-4-NPP TAC should be 12 times larger than in sCO2-HeRo. The dimensions of the scaled-up axial AMB can be then preliminarily calculated by eq. (15). An improvement on this initial design is also implemented by considering the recommendations from "MECOS AG" to obtain a relatively robust scaling-up design from the industrial point of view. Finally, the scaled-up axial AMB for sCO2-4-NPP is shown below with its dimensions, compared with the sCO2-HeRo axial AMB. By considering a large windage loss potentially caused by large radius of the thrust plate, the plate radius is conservatively determined as 67.5 mm.

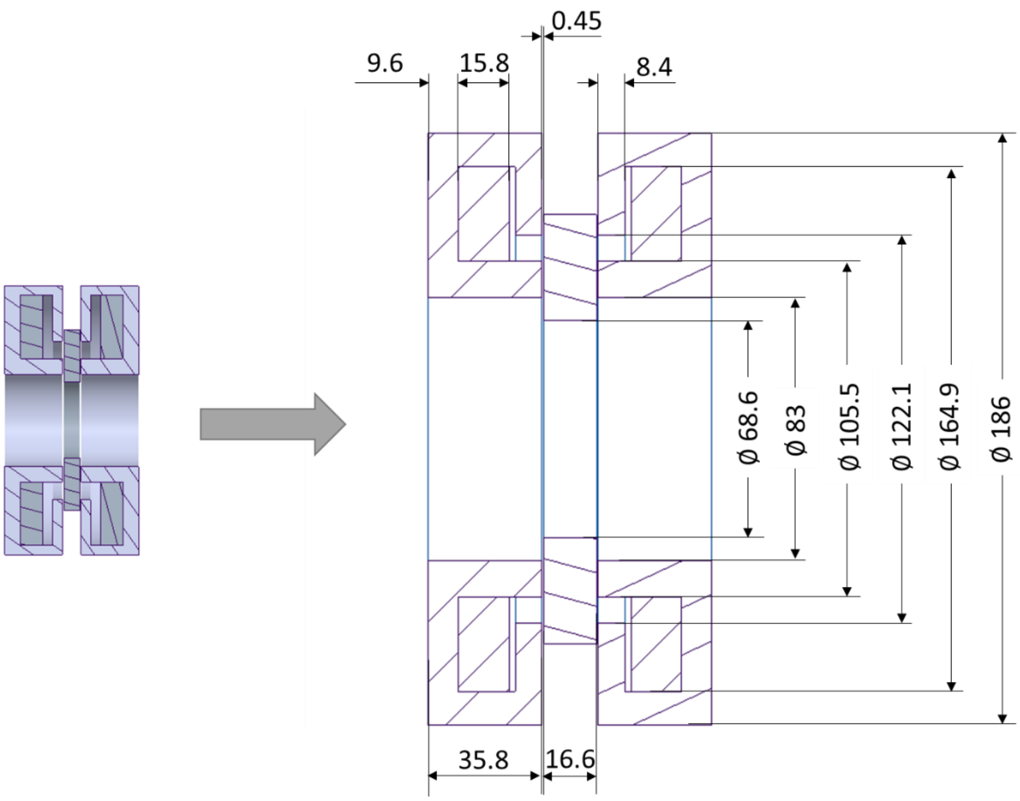

Figure 16: Scaling-up of axial AMB from sCO2-HeRo^{M} to sCO2-4-NPP size (unit in mm)

5.1.3 Safety bearings

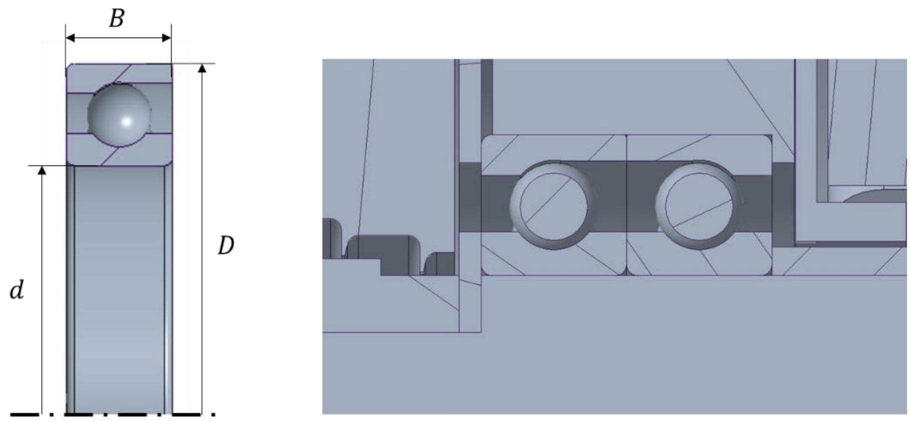

Figure 17: Safety bearing (left) and its X-arrangement (right)

The safety bearings are accessories of the magnetic bearings. They mitigate the potential damage on the machine by taking the extreme loads after the failure of magnetic bearings. Figure 17 (left) illustrates the main dimensions of a safety bearing. Figure 17 (right) shows the X-arrangement of the safety bearings applied in the TAC. Since the safety bearings are special for each application, they are designed by the same supplier of the magnetic bearings (MECOS). Because the outer geometry of the safety bearings used in sCO2-HeRo^{M} is very similar to spindle bearings (e.g., B71904 series from Schaeffler KG), the geometry of the scaled-up safety bearings for sCO2-4-NPP TAC is preliminarily determined to have the same values of a comparable spindle bearing. Finally, the geometry of the safety bearings is extracted from [12] (B71912 series) and are given in Appendix B.3.

5.2 Seals

5.2.1 Seal design

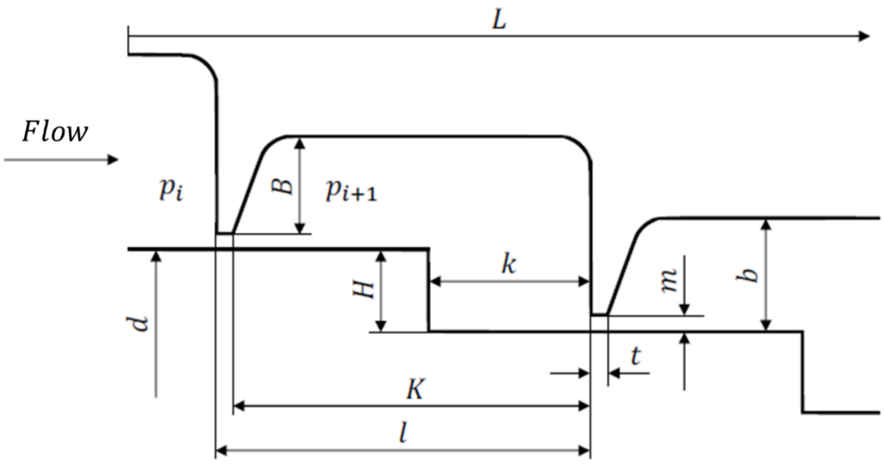

Figure 18: Nomenclature of the seal's dimensions

Figure 18 shows the dimensions of a stepped labyrinth seal which is applied in the sCO2-4-NPP TAC. The width of the radial clearance m between the rotor and the seal's teeth can be estimated by [7] as

$$m = A \cdot \frac{d_m}{1000} + 0.25, \tag{16}$$

where A is an empirical coefficient and d_m denotes the mean diameter of the seal in mm. By considering the mean diameter at the sealing position, the radial clearance is consequently equal to 0.3 mm.

Further, a short calculation in terms of the rotor thermal expansion is implemented to ensure a sufficient radial clearance. Considering the largest radius of the rotor at the sealing position and temperature difference[7] of 60 °C and 267 °C at the compressor and turbine side respectively, the thermal expansion of the rotor can be estimated by

$$\Delta r = r \cdot \alpha \cdot \Delta T, \tag{17}$$

where the symbol α is the thermal expansion factor of the rotor material and equals $11 \cdot 10^{-6}\,K^{-1}$ (value for brass applied for seals). The calculation results finally show thermal expansion of 0.02 mm and 0.1 mm, which are much smaller than the designed radial clearance. This calculation is conservative since the radial clearance is larger than this calculated one when the thermal expansion of the seal and the casing is considered. Thus, the designed radial clearance is sufficient.

Considering the inlet and outlet conditions of the seals and the geometric constraints, further dimensions like the teeth number n, the step height H, the teeth height B, the axial position k, the theoretical length l and the teeth thickness t are obtained. They are given in Appendix B.4, together with their design conditions.

[7] The temperature difference is obtained by subtracting the room temperature (20 °C) with the highest temperature found at the compressor side (80 °C at the compressor impeller discharge) and the turbine side (287 °C at the turbine impeller inlet).

5.2.2 Optimisation option

Swirl break is a well-known method to improve the rotor dynamic behaviour. It can reduce the circumferential velocity of the flow at the seal inlet and, therefore, reduce the swirl inside the flow path. This technology has been applied in sCO2-HeRo^M tested in Essen and applied for the sCO2-4-NPP TAC as well.

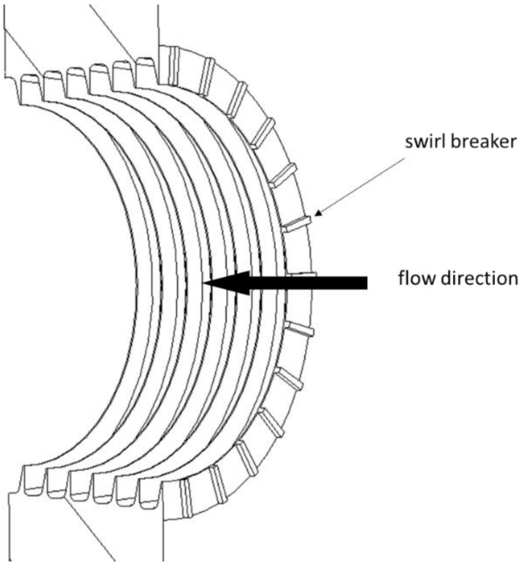

Figure 19: Example of the swirl breaker

5.3 Shaft

The design of the shaft is influenced by several factors such as rotor dynamics, torque and axial length of the components on the shaft. Normally, the shaft can sustain the torque since its relatively large diameter by considering the rotor dynamics. Despite the dominate impact of the rotor dynamics, the basic requirement on the minimum diameter of the shaft is checked in this work. The minimum diameter can be estimate by [13] as

$$d_{min} = \sqrt[3]{\frac{16}{\pi} \cdot \frac{M_d}{\tau_{max}}}, \tag{18}$$

where M_d and τ_{max} denote the shaft torque and the maximum permitted torsional strength. To implement the calculation, the torque and the torsional strength should be known at first. The torsional strength τ_{zul} is normally specified by the material's data sheet once the material applied for the shaft is determined. Following the experience from the sCO2-HeRo TACs, steel 1.4313 (X3CrNiMo13-4) has a good performance. Its strength and resistance against corrosion due to sCO_2 are verified by the experiments. Thus, this material, whose permitted torsional strength is 235 N/mm^2 [14], is applied in sCO2-4-NPP as well. Considered a safety factor of 2.5, the maximum torque can be calculated by

$$M_{d,max} = max\left(\frac{P}{\omega} \cdot 2.5\right), \tag{19}$$

in which P and ω are the power of the turbine and the angular velocity of the shaft including all the calculated operating points corresponding to the performance map shown in Figure 6. Thus, the maximum torque is $1.82 \cdot 10^6$ N·mm. At last, applying eq. (18), the minimum diameter of the shaft is 34 mm. As mentioned before, the practical diameter should be much larger than this minimum one to reach a better rotor dynamic performance and to avoid stress peaks due to a sudden change of the cross-sectional area. Consequently, the actual minimal diameter of the shaft is 50 mm.

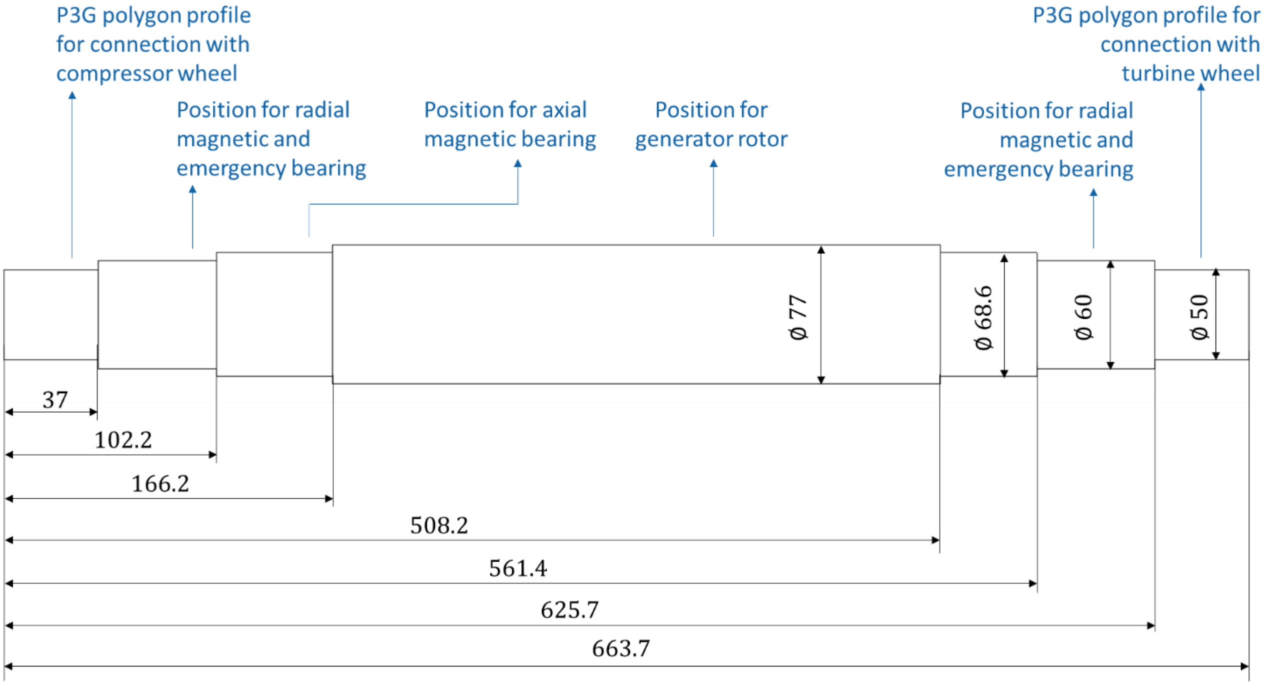

Figure 20: Final design of the shaft specifying the functional positions

The length of the shaft is determined by considering the axial length of the components and the necessary gap width between each other, especially for the stators. To avoid rotor dynamic issues, the shaft is designed as short as possible. Finally, it has a shaft length of around 660 mm by considering position for the compressor, the turbine, the alternator and the bearing sets. A modal analysis is conducted based on the rotor with this shaft design (see section 5.5), and it shows that the rotor will be operated under its first bending mode, namely subcritical. Therefore, the modal analysis verifies the shaft design. The main dimensions and the functional positions of the shaft are specified in Figure 20.

5.4 Casing

Although the turbomachine part is not identified as a safety part in frame of the nuclear regulation, it is still recommended to consider a safety class 2 for such a key component according to WP3 conservatively. Hence, the German nuclear standard "KTA 3211.2" [15] is applied for designing the casing of the sCO2-4-NPP TAC to ensure a robust casing design in nuclear environment. The reason is that the main housing of the TAC can be regarded as a cylindrical pressure vessel, which is described in this standard.

The design of the casing does not start from the inner diameter because the inner contour is not yet fixed and additional space for cables and sensors inside the TAC might be required. Therefore, the outer diameter of the main housing d_{out} is firstly derived from that of sCO2-HeRo^{M} by considering a scaling-up factor of 2.5 based on the diameter ratio between the turbine wheels of both machines. Hence, the main housing of sCO2-4-NPP has an outer diameter of 625 mm. This concept could cause an outer diameter larger than the required (minimum) one. However, it saves more space for the required accessories and more potential to modify or optimise the geometry.

Based on the firstly determined outer diameter, the required wall thickness can be calculated by [15] as

$$s_0 = \frac{d_{out} \cdot p}{2S_m + p} \quad , \tag{20}$$

where p is the pressure at the design point of the pressure vessel in MPa and S_m is a stress comparative value in N/mm^2. By assigning the material to the housing as same as to the shaft, S_m is the minimum between $R_{mN}/4$ and $R_{p0.2N}/1.6$. R_{mN} and $R_{p0.2N}$ are the ultimate stress and the offset yield stress with 0.2 % plastic strain respectively. Finally, this stress comparative value is equal to 195 N/mm^2. Further, the maximum pressure found inside the cylinder cavity of the TAC is at the compressor impeller outlet, which equals 16 MPa. These result in a minimum required wall thickness of 24.6 mm. Considered a safety factor of 2, the wall thickness of the main housing should be larger than 50 mm. Finally, a wall thickness of 100 mm is determined by considering manufacturing of functional surfaces. Similarly, the axial length of the TAC is 960 mm by scaling-up with a factor of 2.7 by comparing the rotor length of both TACs. Finally, the sCO2-4-NPP TAC has outer dimensions as shown below in Figure 21 and Figure 22. They also include the applied flanges, the cable boxes and the additional cooling system. Flanges in PN 160 and PN 250 according to DIN 2501-1 [16] are employed corresponding to the low-pressure side and high-pressure side of the loop respectively. The white components around the main housing are cable boxes. The concrete information of the electrical components is not described in this report. Besides, the pipes with valves shown on the right side build the additional cooling system that is designed for the additional cooling of the magnetic bearing. This system is introduced in section 6.2.

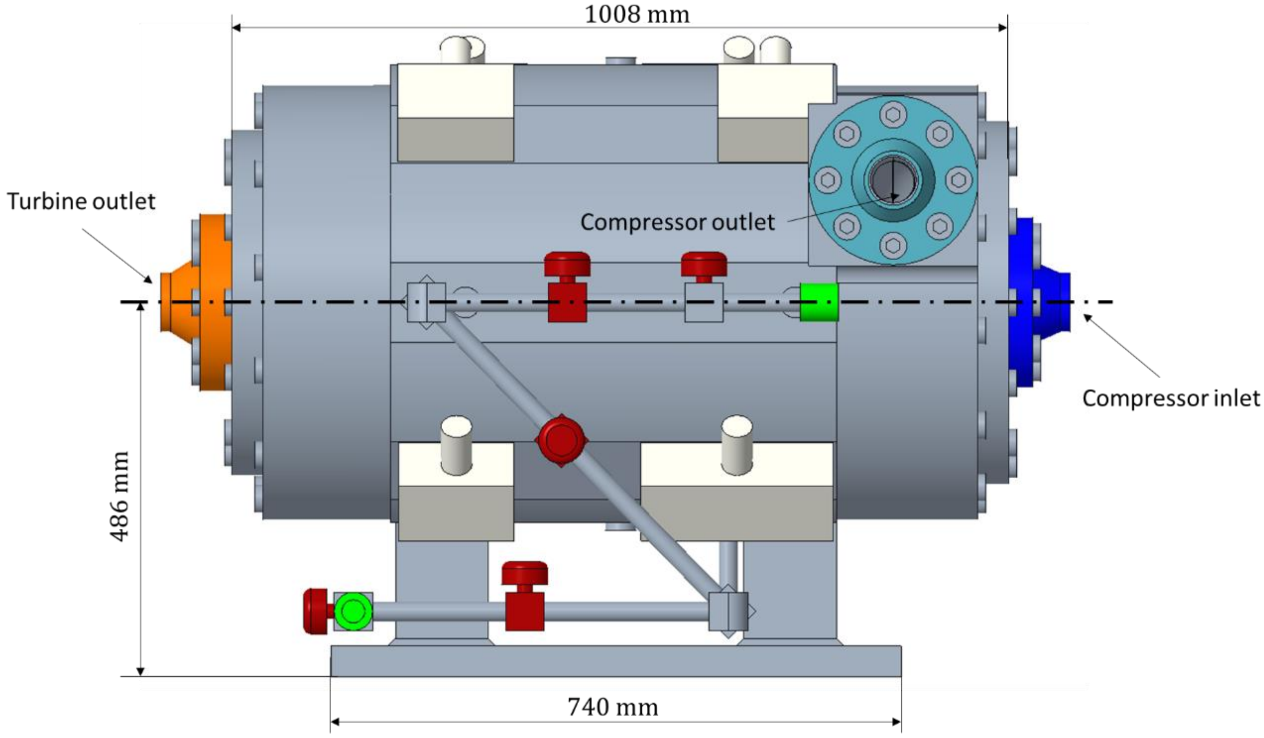

Figure 21: Outer dimensions of the sCO2-4-NPP TAC (front view)

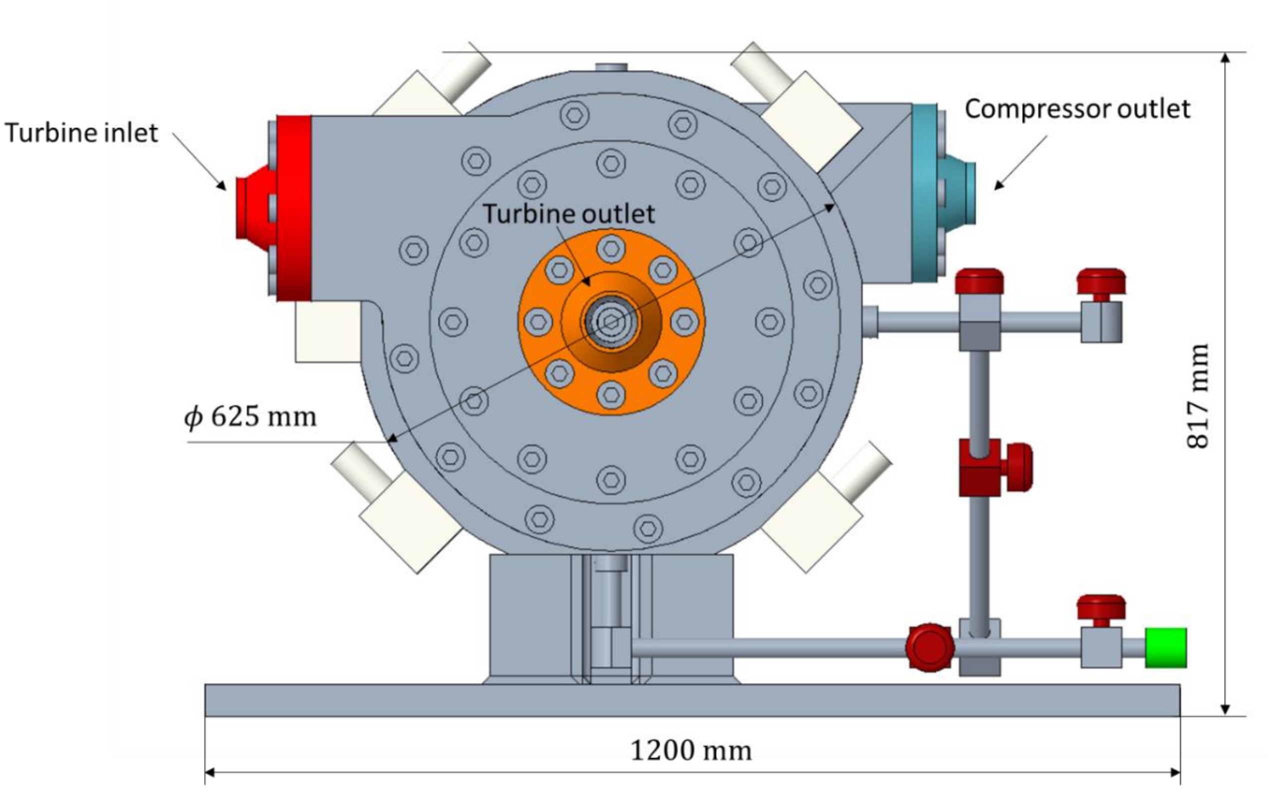

Figure 22: Outer dimensions of the sCO2-4-NPP TAC (left view)

5.5 Rotor dynamics

A modal analysis is conducted to evaluate the rotor dynamic behaviour, where the natural frequencies of the rotor system are calculated. By comparing natural frequencies and rotational speed, the critical speeds can be found, by which the rotor starts vibrating at a relatively high amplitude (resonance). The modal analysis uses the geometry of the rotor shown below, applying the software ANSYS v19.1.

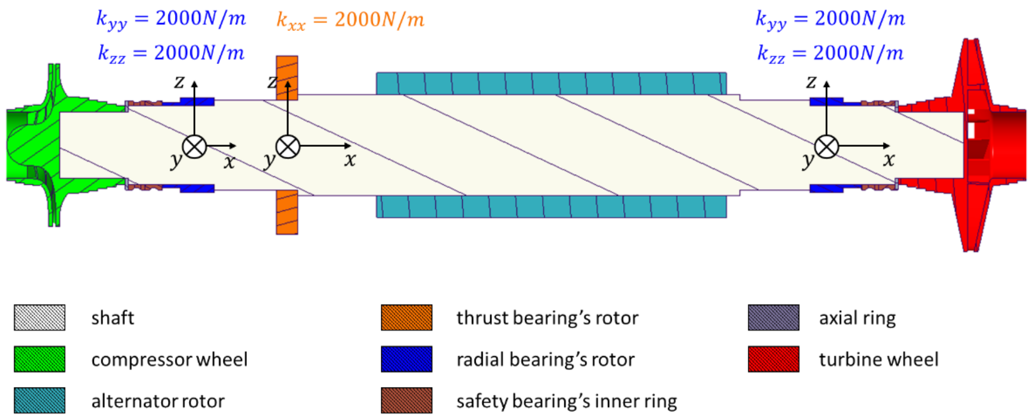

Figure 23: Cross-section view of the rotor's CAD model

Figure 23 exhibits the rotor by assigning parts in different colours. Obviously, the parts dominantly affecting the rotor dynamic behaviour are the compressor wheel (green), the shaft (white), the thrust plate (orange), the alternator's rotor (sky blue), and the turbine wheel (red). The bearing constraints considered are the thrust at the orange position and the radial force at the dark blue positions. According to the final report from MECOS regarding the magnetic bearings designed for the sCO2-HeRo[M], a bearings stiffness of 2,000 N/m is applied for the simulation at free-free conditions. Since the rotor dynamic coefficients of the scaled-up magnetic bearings are not available, this value will be used in the simulation. Besides, materials are also assigned to different parts. Copper (Cu) is applied for the rotor of the alternator according to its data sheet [17], while steel 1.4313 is used for other components. The data sheet is given in Appendix B.5.

Finally, the simulation results in the so-called Campbell-diagram shown below, which exhibits the correlation between frequency vs. rotational speed. The thick black line, known as excitation line, represents the ratio of frequency to the rotational speed equal to 1, where the frequency is equal to the rotational speed. The modal analysis results in the first bending mode of the rotor system at a natural frequency of 692 Hz (N = 0). The mode is split into two modes known as forward whirl (FW) and backward whirl (BW) mode due to the so-called gyroscopic effect, when the shaft speed increases. In other words, both modes are functions of the rotational speed. Finally, two lines (blue and orange) are obtained. Their intersections with the excitation line are denoted by red triangles, where resonance occurs. They are also called the critical speeds of the rotor system in terms of bending mode, which should be avoided in operation. Figure 24 shows that the first critical speed is at 40,000 rpm far away from the turbomachine's design speed and operation range[8], which are denoted by the green circle and transparent blue surface respectively. In another word, the operation of the rotor is much lower than the first critical speed, meaning the rotor is designed sub-critically. Hence, according to the analysis result, the operation of the rotor will never cause rotor dynamic issues.

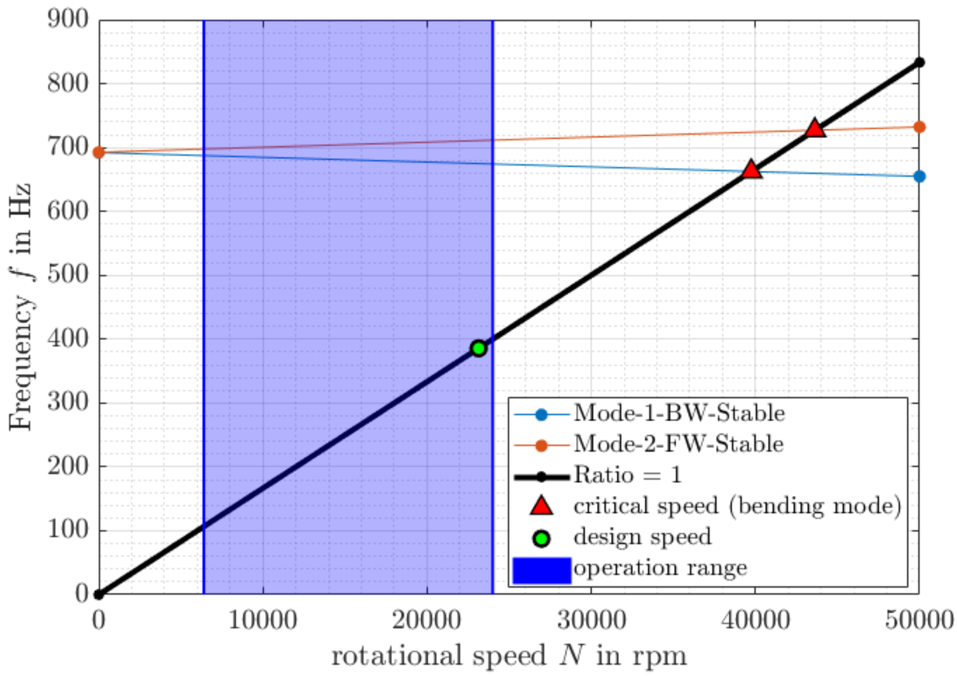

Figure 24: Campbell-diagram for the sCO2-4-NPP rotor

[8] The upper (24,000 rpm) and the lower (6,400 rpm) limit of the operation range correspond to the simulated operation conducted with ATHLET.

6 Auxiliaries

6.1 Alternator

According to the thermodynamic design conditions of the sCO2-4-NPP cycle, the so-called net power (electrical power) obtained from the cycle is about 283 kW at its design point (N = 23 krpm) without considering any mechanical losses. Even by taking into account the losses (leakage and windage loss) introduced in section 4.3.1, the remaining net power still keeps a value of around 200 kW. In the previous research by Hacks et al. [18], recommendation is made about different sizes of the alternator, in which the type "mW 17/25-4-s2r5" from "e+a Elektromaschinen und Antriebe AG" is appropriate for a rotational speed of 23.3 krpm and a rated output power of 210 kW [17], fulfilling all the requests from the design. Therefore, this alternator is selected for the sCO2-4-NPP TAC. It is an asynchronous 4-pole alternator, whose data sheet and performance characteristics are given in Appendix B.5. A sketch of the alternator is shown below to illustrate the dimensions corresponding to the data sheet.

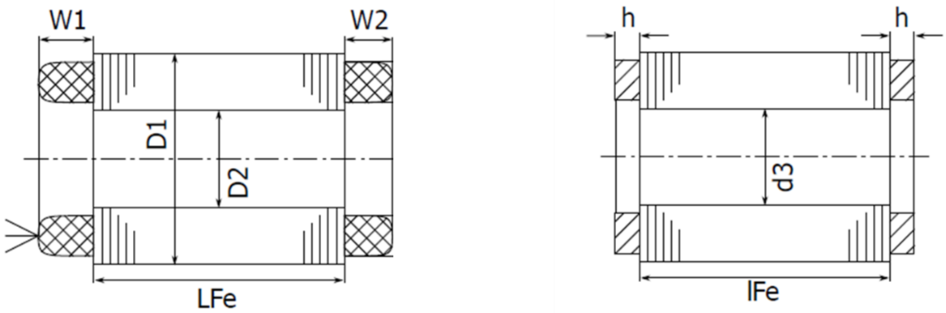

Figure 25: Sketch of the alternator [17] (left: stator; right: rotor)

6.2 Additional cooling system

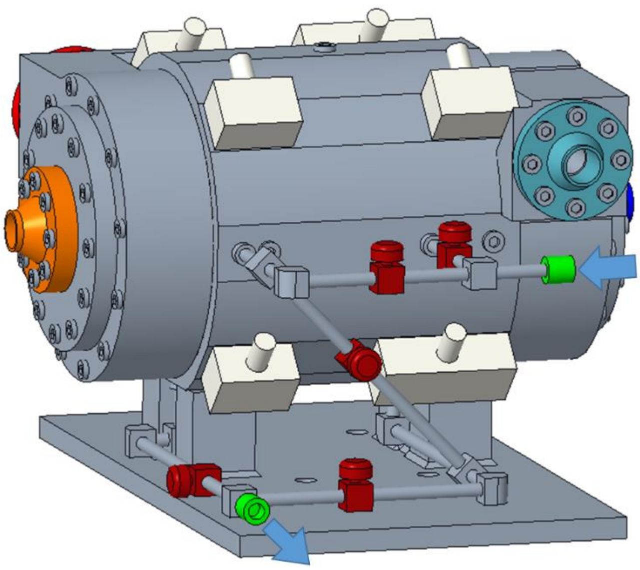

Figure 26: Outer view of sCO2-4-NPP TAC including the additional cooling system

Based on the experience from sCO2-HeRo[M], the additional cooling system is built as shown in Figure 26, where the green positions are the interfaces between the TAC and the sCO_2 loop and the blue arrows show the direction of the additional cooling flow. The red buttons are valves to control the cooling flow rate. The motivation to build this system is that the AMBs applied in sCO2-HeRo[M] have a temperature limit of 150 °C to 200 °C. The challenge is the high temperature at the turbine side because the turbine's inlet temperature is about 200 °C and the hot sCO_2 flows towards the radial AMB (RAMB) and the alternator (A/G) via the turbine's shaft seal (L), as shown in Figure 27. However, this issue becomes more significant in sCO2-4-NPP TAC due to the higher temperature (287 °C) at the turbine inlet. This cooling system allows a direct cooling of this hot flow by introducing the cold flow from the compressor outlet. The blue arrow in front of valve 29 is the inflow of the cooling system, corresponding to the arrow at the system inlet shown in Figure 26. Considering the temperature constraint of the radial AMB (200 °C) and the alternator (145 °C), the sCO2-4-NPP TAC will probably need this system.

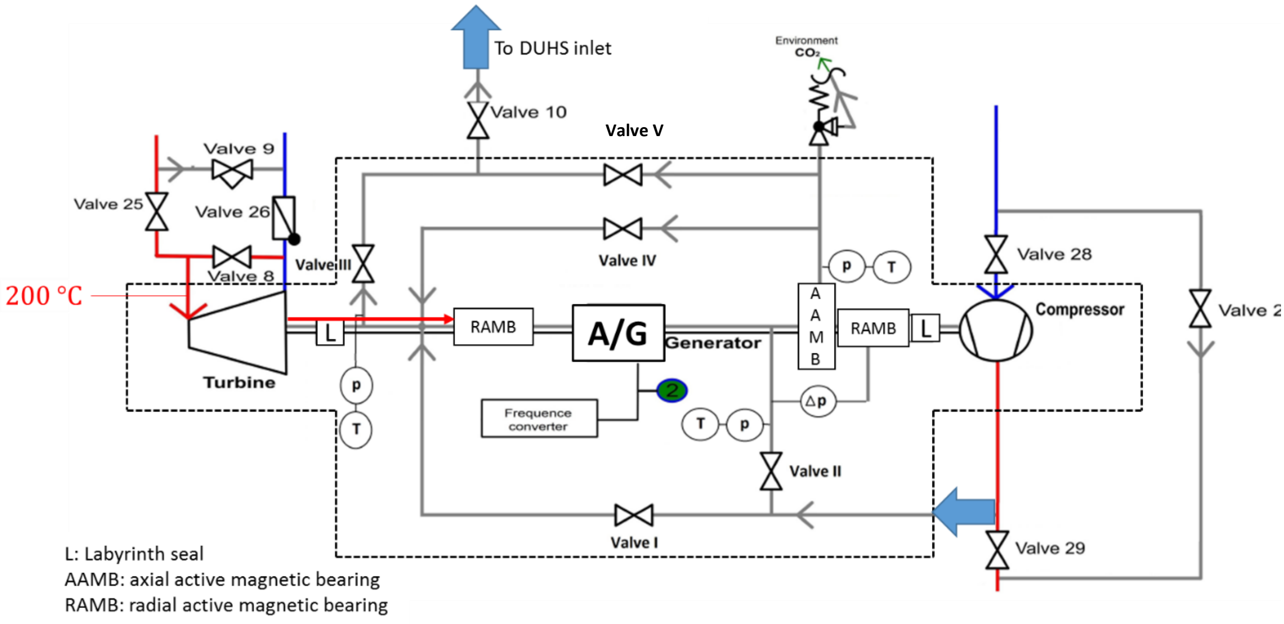

Figure 27: P&ID diagram of the additional cooling system

The cooling flow is extracted from the compressor outflow before it reaches valve 29 and then led to the rotor via valve I and II. Simultaneously, there are leakage flows from the shaft seals (L) at both compressor and turbine side. Finally, the cooling flow and the leakage flows are mixed in the system and discharged via valve 10. Since there are five valves set in the system to control the inflows and outflows, various cooling concepts can be achieved by combining different valves. This design allows the adjustment of the system in different environmental conditions (requirement in high or low cooling power). However, opening valve I and V is recommended by considering the experience of the tests in Essen, by which cold flow from the compressor discharge is directly led to the outlet of the turbine's shaft seal to cool the hot leakage from the turbine. The flows are firstly mixed and then used for cooling the radial AMB and the alternator. Finally, the coolant is discharged via valve V and 10. There are three reasons to apply this concept. The first one is that the cooling effect can be achieved by providing enough cold flow (the calculation concept is described in Appendix A.2). The second one is that this concept can reduce the thrust on the thrust bearing (AAMB) because of the centrifugal flows at both side of the thrust plate. The third one is that a relatively low density of sCO_2 inside the generator gap is preferred rather than high density since high density can cause rotor dynamic issue. On the other hand, the additional cooling causes a "leakage" of the sCO_2 loop directly after the compressor, which influences the mass flow rate in subsequent components (CHX and turbine) and the power of the TAC. The corresponding analysis is described in section 4.3.1.2.

6.3 Piston pump for cold start-up

In order to start-up the TAC from cold standstill, a piston pump is used to circulate CO_2 in the sCO2-HeRo loop to slowly heat the fluid up in a heater and bring it in the whole loop to a supercritical state (over 74 bar and 31°C). The main reason is the inhomogeneous fluid properties (two-phase CO_2) in the TAC cavity before the loop is operated. The inhomogeneous distribution of CO_2 prevents the lift-up of the rotor. The piston pump helps to distribute the liquid and gaseous CO_2 evenly in the loop as well as in the TAC.

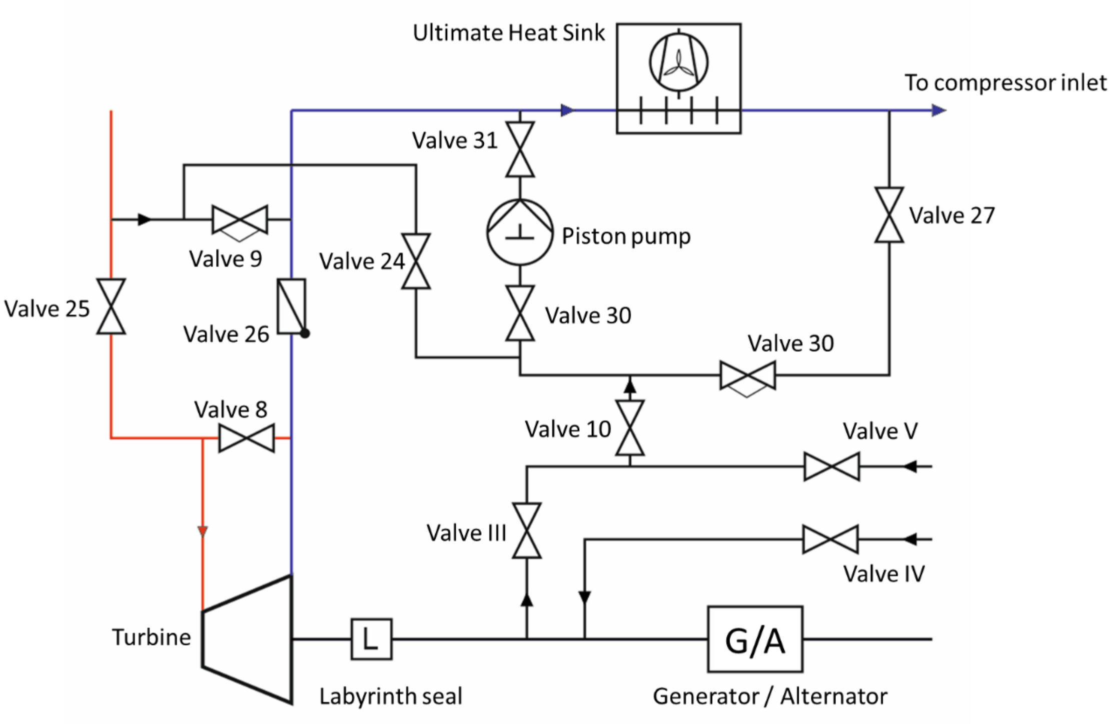

Figure 28: P&ID diagram including the piston pump

As shown in Figure 28, the inlet of the piston pump is connected to the TAC through valve 10, which is also shown in Figure 27. The outlet of the piston pump is connected with the pipe (blue) between the turbine outlet and the UHS inlet via valve 31. This results in a leakage flow through the shaft seal (L) of the turbine, which is used to warm up the TAC. After the CO_2 in the loop is supercritical and ready for the operation, the rotor is lifted-up and rotates at low rotational speed. Subsequently, the compressor takes the task of the piston pump and the latter is shut down. Task 4.1 (D4.1) has provided the available operation strategy for a cold start-up.

7 Conclusion

In the EU project sCO2-4-NPP, a sCO_2 heat removal system based on the Joule cycle has been designed for the NPPs in Europe. UDE has designed the turbomachine of the sCO_2-Joule-cycle in the frame of task 4.2 and reported the conceptual design in this deliverable.

In this task, a mean-line tool is established to predict the performance of the turbomachine and validated with the experimental and numerical results in terms of the sCO2-HeRo^{M}. The generated performance maps are delivered to the simulation teams working in WP2 and WP5. In addition, generator loss and leakage loss are considered and analysed. Both the tool and the performance maps are exploitable for further development of the sCO2-Joule-cycle technology as well as for other applications. Furthermore, the main dimensions of the turbomachine and its components are specified. This supports the designer in building the final architecture of the cycle modules in NPPs as well as bringing the first impression to the public of how a TAC could look regarding the sCO_2 heat removal system in scale of real NPP.

Consequently, the design includes firstly the aerodynamic design and its off-design where the performance maps of the most important parts, namely the compressor and the turbine, are generated. The performance maps are applied as turbomachine model in the simulations with the thermodynamic codes (ATHLET, CATHARE and Modelica), and in turn, the cycle simulation results indicate that the aerodynamic design has fulfilled the requirements. Losses due to the disk friction of the generator as well as the leakage and the additional cooling flow are evaluated and described in this report, to show their impact on the net power of the TAC. Secondly, the mechanical design of the TAC closely follows the design concept of the sCO2-HeRo^{M} by considering reasonable scaling-up factors. Simultaneously, recommendations and regulations from the industrial or nuclear aspects are taken into account. The design concepts of the important mechanical parts like bearings, seals, shaft and the casing are finally specified. In addition, modal analysis is conducted to research the rotor dynamic behaviour preliminarily. The result indicates a subcritical design, verifying a robust rotor dynamic behaviour. Thirdly, the auxiliaries of the TAC are introduced, whose effect and impact on the TAC and the whole cycle module are described. Finally, the sCO2-4-NPP TAC is shown below.

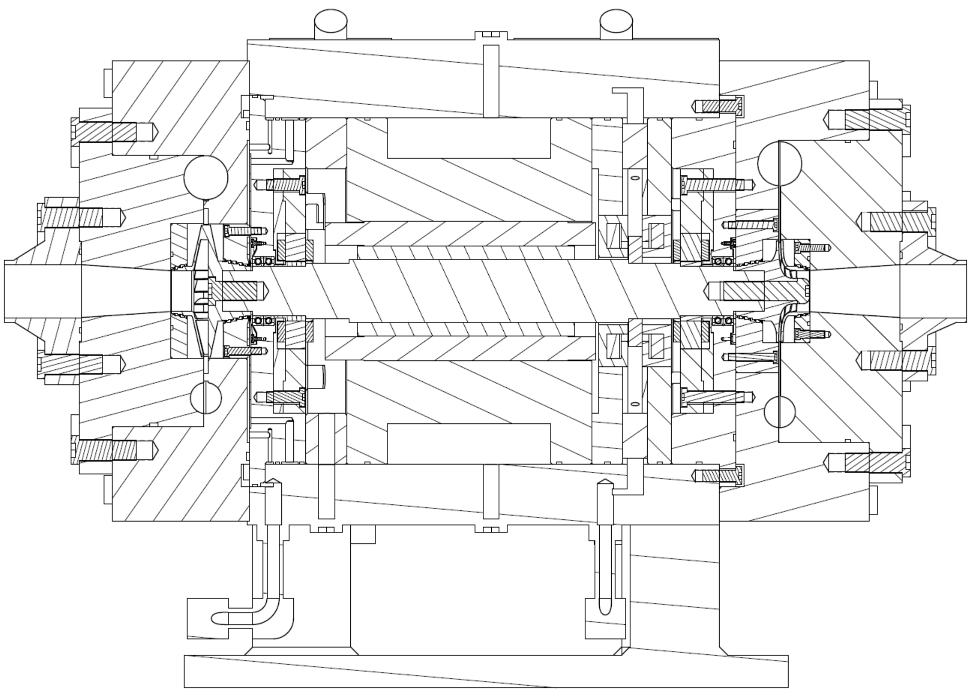

Figure 29: sCO2-4-NPP TAC (cross-section view)

Standards considered during the design are “KTA 3211.2” [15] and “API 617” [19]. Although none of regulations regarding the TAC are specified in nuclear standards, it is still recommended to consider a safety class 2 for such a key component according to WP3. Therefore, the German nuclear standard “KTA 3211.2” is applied for the turbomachine’s casing. The design of other parts has followed the industrial standard “API 617”. Further qualification methods of the TAC are developed in the parallel task 4.6 and finally reported in D4.7.

8 References

[1] J. Venker, „Development and Validation of Models for Simulation of Supercritical Carbon Dioxide Brayton Cycles and Application to Self-Propelling Heat Removal Systems in Boiling Water Reactors," Institut für Kernenergetik und Energiesysteme (IKE), Universität Stuttgart, 2015.

[2] I. Abd El Hussein, A. J. Hacks, S. Schuster und D. Brillert, „A Design Tool for Supercritical CO2 Radial Compressors Based on the Two-Zone Model," in *Proceedings of ASME Turbo Expo 2020, Turbomachinery Technical Conference and Exposition*, London, England, 2020.

[3] H. Ren, A. J. Hacks, S. Schuster und D. Brillert, „MEAN-LINE ANALYSIS FOR SUPERCRITICAL CO2 CENTRIFUGAL COMPRESSORS BY USING ENTHALPY LOSS COEFFICIENTS," in *4th European supercritical CO2 Conference*, March 23-24, 2021, Online, 2021.

[4] S. Schuster, C. N. Markides und A. J. White, „Deisgn and off-design optimisation of an organic Rankine cycle (ORC) system with an integrated radial turbine model," *Applied Thermal Engineering,* pp. Volume 174, 115192, 25 June 2020.

[5] A. Hacks, S. Schuster und D. Brillert, „Stabilizing Effects of Supercritical CO2 Fluid Properties on Compressor Operation," *Int. J. Turbomach. Propuls. Power,* pp. Vol. 4(3), 20, 2019.

[6] W. Bohl und W. Elmendorf, Strömungsmaschinen 1: Aufbau und Wirkungsweise, Würzburg, Germany: Vogel, 11. Auflage 2013.

[7] W. Bohl, Strömungsmaschinen 2: Berechnung und Konstruktion, Vogel, 2013.

[8] E. Bilgen und R. Boulos, „Functional Dependence of Torque Coefficient of Coaxial Cylinder on Gap Width and Reynolds-Numbers," *Journal of Fluids Engineering,* pp. 95(1), 122-126, 1973.

[9] J. Betancor, M. N. Sahinkaya und Y. H. Zweiri, „Radial Active Magnetic Bearing Design Optimization," in *IFToMM 2018*, pp 321-334, 2019.

[10] G. Barbaraci, G. V. Mariotti und A. Piscopo, „Active magnetic bearing design study," *Journal of Vibration and Control 19 (16),* pp. pp. 2491 - 2505, 12 July 2012.

[11] G. Barbaraci, „Axial active magnetic bearing design," *Journal of Vibraion and Control,* pp. 1-8, 13 May 2014.

[12] SCHAEFFLER GRUPPE INDUSTRIE, Wälzlager, Herzogenaurach, Schweinfurt: Schaeffler KG, 2008.

[13] C. Pfleiderer und H. Petermann, Strömungsmaschinen, 7., unveränderte Auflage, Germany: Springer, 2005.

[14] H. Wittel, D. Muhs, D. Jannasch und J. Voßik, Roloff/Matek Maschinenelemente: Tabellenbuch, Germany: Springer, 2009.

[15] *KTA 3211.2 Druck- und aktivitätsführende Komponenten von Systemen außerhalb des Primärkreises, Teil 2: Auslegung, Konstruktion und Berechnung,* 2013-11.

[16] DIN2501-1, „DIN 2501-1:1972-02 : Flansche; Anschlußmaße (Flanges; Connecting Dimensions),“ Beuth, Germany, 1972-02.

[17] e+a Elektromaschinen und Antriebe AG, *Asynchron-Elan Typen 4-polig,* 2018.

[18] A. Hacks und D. Brillert, „Scaling consideration for the application of the sCO2-HeRo system in nuclear power plants,“ in *2nd European supercritical CO2 Conference*, Essen, Germany, 2018.

[19] Energy API, American Petroleum Institute, *Axial and Centrifugal Compressors and Expander.compressors (API Standard 617) 8.Edition,* Washington, DC: API Publishin Services, 2014.

[20] H.-S. Pham, N. Alpy, J.-H. Ferrasse, O. Boutin, M. Tothill, J. Quenaut, O. Gastaldi, T. Cadiou und M. Saez, „An approach for establishing the performance maps of the sc-CO2 compressor: Development and qualification by means of CFD sumulations,“ *International Journal of Heat and Fluid Flow, Elsevier,* pp. 61 (Part B), pp.379-394, 2016.

[21] K. Lüdtke, Process centifugal compressors: basics, function, operation, design, application., Springer Science & Business Media, 2004.

[22] R. H. Aungier, Centrifugal Compressors: A Strategy for Aerodynamic Design and Analysis., New York: ASME, 1999.

[23] T. W. Ha, „Rotordynamic analysis for stepped-labyrinth gas seals using Moody's friction-factor model,“ *KSME International Journal,* pp. Vol.15, No.9, pp. 1217-1225, September 2001.

[24] K. Leeb, „Experimentelle und numerische Untersuchungen zum Durchflußverhalten von Labyrinthdichtungen von Turbomaschinen unter dem Einfluß von Rotation, Wellendeaxierung und Drall der Zuströmung,“ Wien, 1997.

[25] V. Schramm, Labyrinthdichtungen maximaler Dichtwirkung, Berlin : Logos Verl., 2011.

[26] B. M. Trojanovsky, „Der Dampfverlust durch Labyrinthstopfbüchsen,“ Band 1, Mitteilung des WTI, 1950.

[27] A. Egli, „The Leakage of Steam Through Labyrinth Seals,“ in *Transactions of the American Society of Mechanical Engineers*, 57(3), S.115-122, 1935.

[28] D. a. M. G. Rhode, „Design optimisation and testing of a pump wear ring labyrinth seal.,“ *Reston, Virigina: American Institute of Aeronautics and Astronautics,* pp. S.1685-1692, 1988.

[29] X. Yan, J. Li und Z. Feng, „Effects of sealing clearance and stepped geometries on discharge and heat transfer characteristics of stepped labyrinth seals,“ *Proceedings of the Institut of Mechanical Engineers, Part A: Journal of Power and Energy,* pp. 225(4), S.521-538, 2011.

[30] K. a. D. W. C. Miyake, „Leakage characteristices of labyrinth seal,“ *Journal of the Chinese Society of Mechanical Engineers,* pp. Ausgabe 11, S.334-348, 1990.

[31] H. Yuan, S. Pidaparti, M. Wolf, J. Edlebeck und M. Anderson, „Numerical modeling of supercritical carbon dioxide flow in see-through labyrinth seals,“ *Nuclear Engineering and Design,* pp. Ausgabe 293, S.436-446, 2015.

Appendix A Calculation Methods

A.1 Corrected values

The pressure ratio and the mass flow rate are given in corrected values calculated by [20] as

$$\dot{m}_c = \left(\dot{m}\frac{\sqrt{n_s ZRT}}{n_s p}\right)_a \left(\frac{n_s p}{\sqrt{n_s ZRT}}\right)_{ref} = \left(\dot{m}\frac{1}{\rho c}\right)_a (\rho c)_{ref}, \tag{21}$$

$$N_c = \left(N\frac{1}{\sqrt{n_s ZRT}}\right)_a \left(\sqrt{n_s ZRT}\right)_{ref} = \left(\frac{N}{c}\right)_a (c)_{ref}, \tag{22}$$

$$\Pi_c = \left[\frac{n_{s,ref}-1}{n_{s,a}-1}\left(\Pi_a^{\frac{n_{s,a}-1}{n_{s,a}}} - 1\right) + 1\right]^{\frac{n_{s,ref}}{n_{s,ref}-1}}, \tag{23}$$

where n_s, p, Z, R, T, ρ and c are ratio of the specific heat capacities, pressure, compressibility factor, specific gas constant, temperature, density and speed of sound respectively, while the subscripts a and ref represent the actual conditions and the reference condition respectively. The reference condition is p_1 = 126 bar, T_1 = 55 °C for the compressor and p_3 = 126 bar, T_3 = 287 °C for the turbine.

A.2 Modelling of the additional cooling system

A.2.1 Modelling method

According to the tests conducted in Essen, a concept of operating the additional cooling system for the magnetic bearing is specified, shown with the green path in Figure 30.

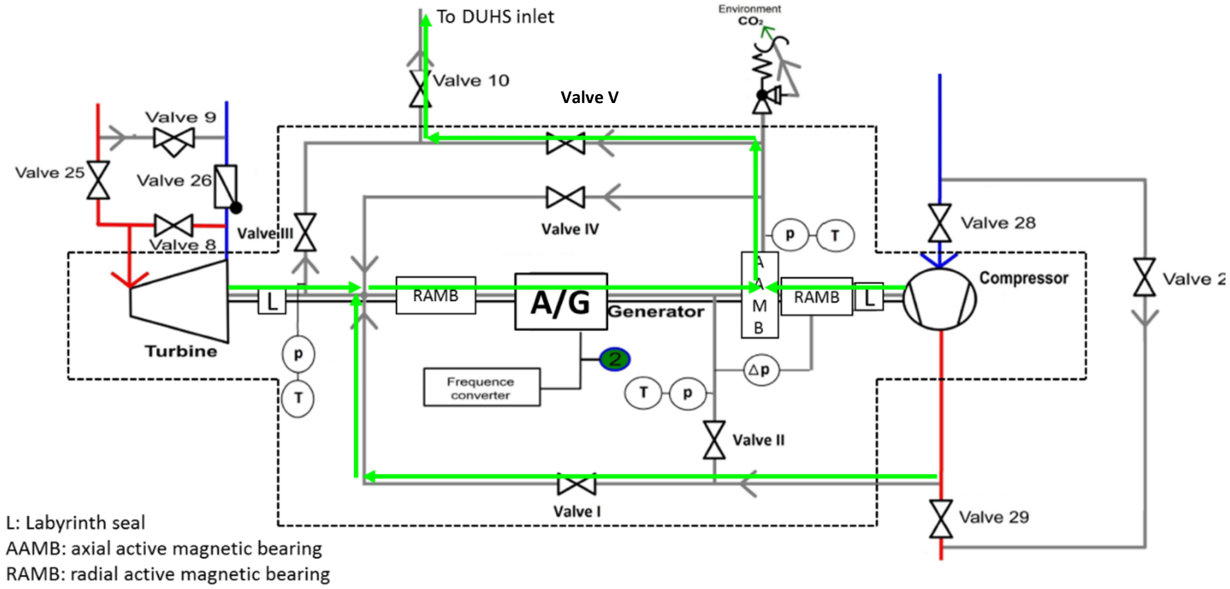

Figure 30: P&ID diagram for additional cooling system of the TAC

The cold flow from the compressor outlet can directly cool the hot seal leakage from the turbine side, which could be over 250 °C in case of sCO2-4-NPP, before the hot flow reaches the radial AMB (RAMB) at the turbine side. Since extraction of the cooling flow from the compressor outlet influences the inlet mass flow of the turbine, it is important to know how much mass flow rate is transported by the cooling system. To achieve this goal, the system will be first modelled.

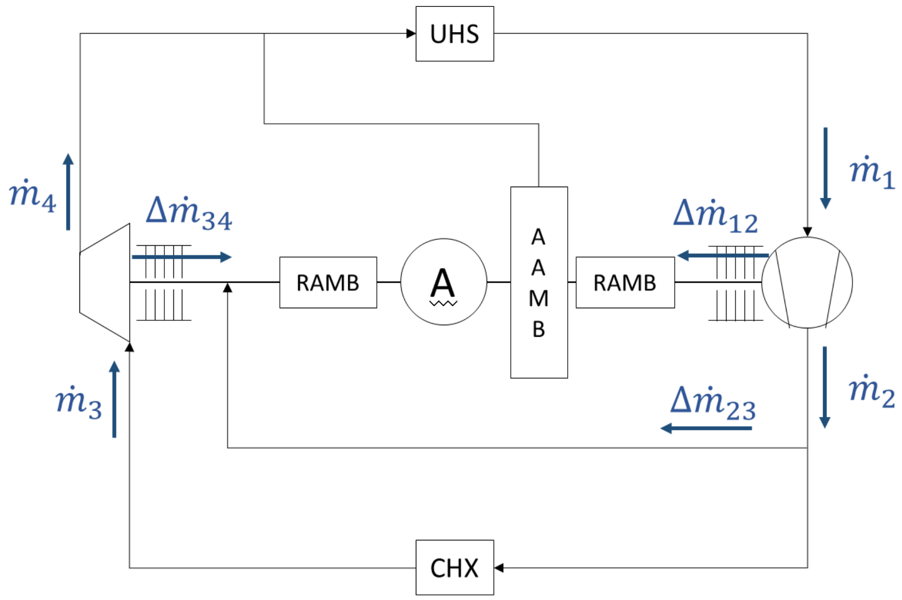

Figure 31: Simple model of the cooling system

Figure 31 shows a simple model of the cycle module, where the mass flow balance within the module is presented as well. Since the only parameters influencing the performance maps of the TAC are the inlet mass flow rates $\dot{m}_1$ and $\dot{m}_3$, the most important leakage flows are $\Delta\dot{m}_{12}$ and $\Delta\dot{m}_{23}$ from the compressor's shaft seal and outlet respectively. The cooling flow $\Delta\dot{m}_{23}$ is mixed with the hot leakage $\Delta\dot{m}_{34}$ from the turbine's shaft seal, and their mixture is led to the radial AMB and the alternator (A). The required cooling flow rate $\Delta\dot{m}_{23,req}$ is defined as the minimum mass flow rate required for cooling the radial AMB and the alternator. The leakage ratio of the loop is then expressed by

$$lr = \frac{\Delta\dot{m}_{12} + \Delta\dot{m}_{23,req}}{\dot{m}_1} = \frac{\dot{m}_1 - \dot{m}_3}{\dot{m}_1}. \tag{24}$$

To estimate the required cooling flow $\Delta\dot{m}_{23,req}$, the heat transfer within the radial AMB at the turbine side and the alternator is modelled, where each component is regarded as an adiabatic system including its stator and flow path, as shown in Figure 32. The dark blue dashed lines draw the border of the components. The total system has an inlet (in) at the radial AMB's inlet and an outlet (out) at the alternator's outlet. The space between the radial AMB and the alternator is neglected and it is assumed that the boundary condition at the radial AMB's outlet and the alternator's inlet is identical. In the radial AMB, the electrical power is totally converted into heat $\dot{Q}_{MB}$ since this energy does not work on the radial AMB itself. In contrast, the alternator exploits the major part of its electrical power and only a minor part of this power is converted into heat. The ratio depends on the efficiency of the alternator. By assuming an efficiency of 95 %, the produced heat $\dot{Q}_G$ is about 5 % of the alternator's power. For both components, the rotating rotor does work (P_{MB} and P_G) on the fluid, which is regarded as the friction power, also called windage loss, due to relative movement between the rotor and the fluid. This power can be calculated by eq. (4). In a relatively conservative estimation, it can be assumed that all the heat and power produced by the radial AMB and 5% of the alternator are transmitted into the fluid.

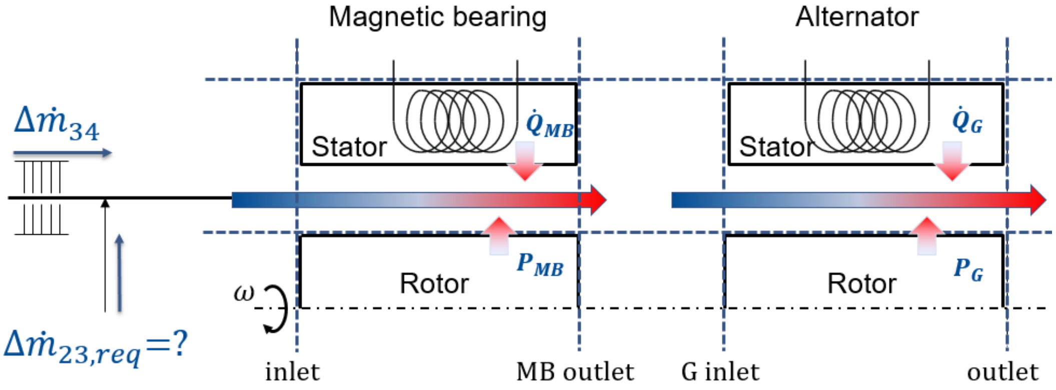

Figure 32: Modelling of the heat transfer regarding the radial AMB and the alternator

According to Figure 32, there is

$$P_{MB} + \dot{Q}_{MB} = \left(\Delta\dot{m}_{34} + \Delta\dot{m}_{23,req}\right) \cdot c_p \cdot \left(T_{MB,out} - T_{in}\right), \tag{25}$$

$$P_G + \dot{Q}_G = \left(\Delta\dot{m}_{34} + \Delta\dot{m}_{23,req}\right) \cdot c_p \cdot \left(T_{out} - T_{G,in}\right), \tag{26}$$

in which c_p and T are the isobaric heat capacity and the temperature of the fluid. In this case, the difference of the velocity between the inlet and the outlet is neglected. Obviously, the cooling flow $\Delta\dot{m}_{23,req}$ is mixed with the leakage flow $\Delta\dot{m}_{34}$ from the turbine's shaft seal and then the mixture moves through the flow path of the components. The mixing of these two flows is calculated by considering the energy conservation. Finally, by assuming an outlet temperature T_{out}, the total mass flow $\Delta\dot{m}_{34} + \Delta\dot{m}_{23,req}$ can be calculated. This outlet temperature is equal to the maximum temperature of the alternator since the fluid does not provide any heat removal with a higher temperature. A conservative estimation of the alternator's maximum temperature is 145 °C according to "e+a Elektromaschinen und Antriebe", the alternator manufacturer for the sCO2-HeRo TACs. Because the maximum temperature of the radial AMB[9] is higher than the alternator's and the cooling flow has lower temperature within the radial AMB's cavity, the temperature limit of the radial AMB is not considered in the calculation.

After the cooling flow $\Delta\dot{m}_{23,req}$ is estimated, the leakage ratio lr can be calculated, where the leakage flows ($\Delta\dot{m}_{12}$ and $\Delta\dot{m}_{34}$) from the compressor and turbine's shaft seal are needed as well. The calculation of these leakage flows is based on the model by Lüdtke [21] as

$$\dot{m}_{lk} = \zeta \cdot A \cdot \varepsilon \cdot \sqrt{p_{in}} \cdot \sqrt{\rho_{in}}, \tag{27}$$

where $\zeta \cdot A$ is called seal factor and specified as 0.0009 by considering the seal area A, ε is seal coefficient and is a function of the fin number and the pressure ratio of the labyrinth seal. p_{in} and ρ_{in} are the pressure and density of the fluid at the seal inlet. They can be calculated by employing the model of pressure drop in rotating cavity according to Aungier [22] as

[9] The temperature limit of the radial AMB is specified by the magnetic bearing manufacturer „MECOS“, who has designed and produced the magnetic bearings for sCO2-HeRo[M] in sCO2-4-NPP task 4.1.

$$\Delta p = p_2 - p_{in} = K^2 \omega^2 \rho r \cdot \Delta r, \tag{28}$$

where r is the radius, ω is the angular velocity and K is the clearance gap swirl parameter. p_2 is here the impeller outlet pressure. Based on eq. (27) and (28), the leakage ratio of the compressor ($\Delta\dot{m}_{12}/\dot{m}_1$) and the turbine ($\Delta\dot{m}_{34}/\dot{m}_3$) can be calculated and finally specified by Figure 33, where the operating line is exhibited as well. From the start point, namely the maximum load of the module, the compressor is operated with a declining leakage ratio from about 2.6 % to 1.5 %, while the turbine has an increasing leakage ratio from 0.5 % up to 2.9 %. These calculation results are used for the calculation conducted in section 4.3.1.2 since it considers the corresponding simulated data.

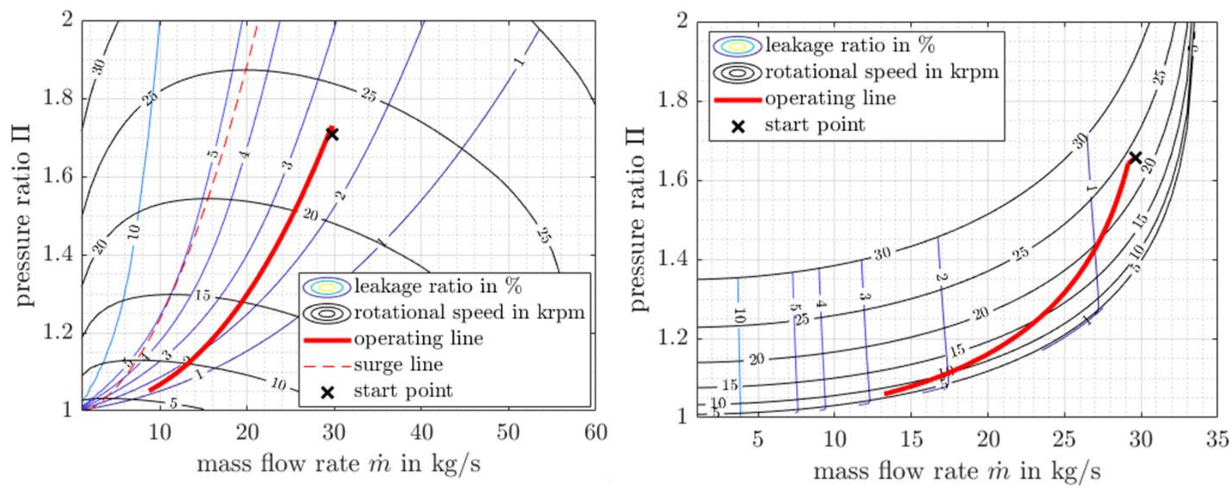

Figure 33: Performance maps of leakage ratio regarding the compressor (left) and the turbine (right) including the operating line

A.2.2 Verification

To verify the calculation model, one of the experimental results regarding the sCO2-HeRo[M] is taken into account. In this case, the leakage via the compressor's shaft seal firstly flows through the radial AMB at the compressor side, the axial AMB (AAMB), the alternator as well as the radial AMB at the turbine side, and subsequently mixed with the additional cooling flow. Finally, they are mixed with the hot leakage from the turbine's shaft seal and led back to the loop via valve III and 10, as shown in Figure 34. Consequently, the temperature at the orange position will be calculated and compared with the measured one.

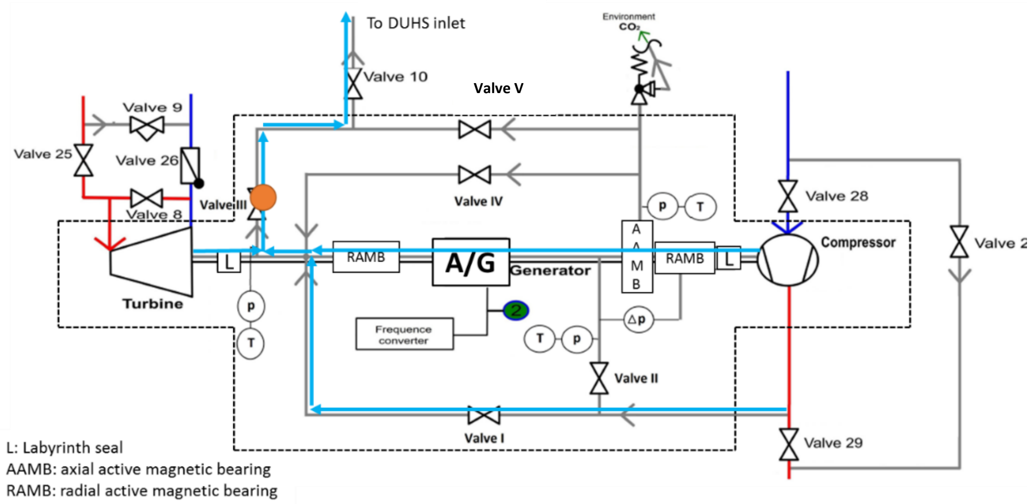

Figure 34: Experimental case for verification of the model

Unfortunately, the leakages were not directly measured. They are calculated with the empirical leakage factors obtained in the tests. By assuming a leakage ratio of 10 % at the turbine's shaft seal, the calculation results in the blue curve exhibited in Figure 35, where the orange curve denotes the measured temperature. The temperature drop found with the blue curve at 16:28 is due to the further opening of valve I from 5 % to 7.5 %. In contrast, the orange curve has a relatively shallow fluctuation and a smoother course since the sensor collects the temperature over time and returns the mean value, while the calculation is conducted for each operating point and therefore more sensitive. However, the trend of both curves shows a plausibility of the calculation results, verifying the reasonableness of the model for a conservative estimation.

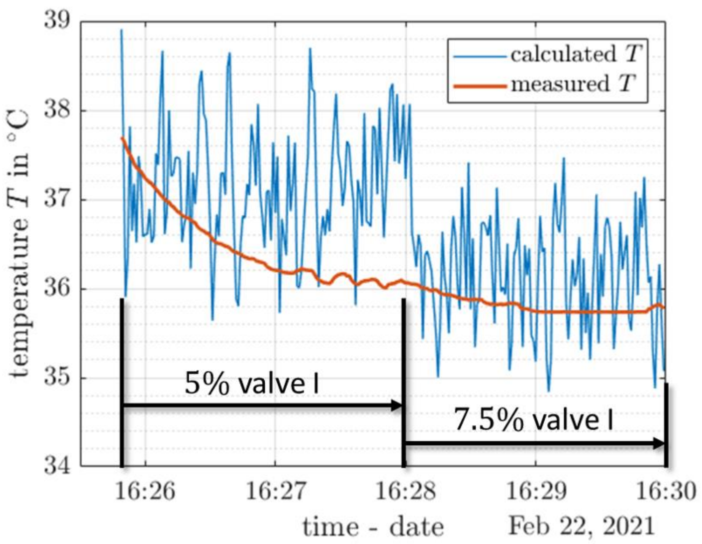

Figure 35: Comparison between the calculated and measured temperature at valve III

Appendix B Technical information

B.1 Compressor's blade parameters

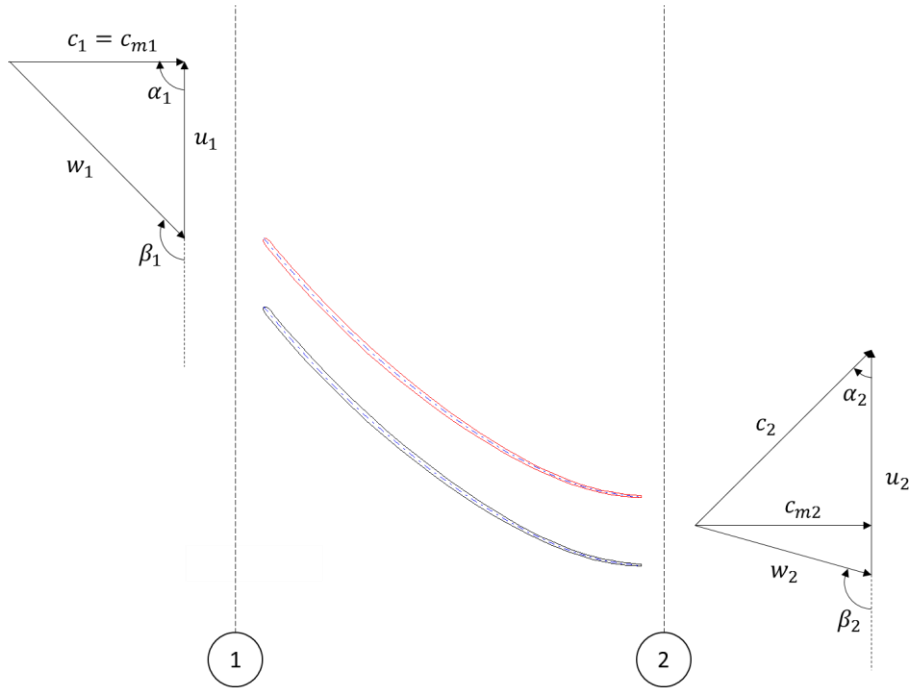

Figure 36: Velocity triangles of the compressor impeller (1: leading edge; 2: trailing edge)

Figure 36 illustrates the velocity triangles at the design point at the leading edge and the trailing edge of the compressor's impeller in blade-to-blade view, where c, w, u, c_m, α and β represent the absolute flow velocity, the relative flow velocity, the circumferential velocity, the meridional flow velocity, the absolute flow angle and the blade angle, respectively. It helps to understand the corresponding parameters of the blades. For calculating the blade angle at the leading edge, it is assumed that $\alpha_1 = 90\,°$ or $c_1 = c_{m1}$, which indicates a swirl-free inflow at the leading edge. The blade angle at the trailing edge is selected for having a low sensitivity of the efficiency to the mass flow rate, to guarantee a relatively wide operation range. The information of the blade's parameters is shown below:

Parameter	Symbol	Unit	Value
Blade angle at leading edge (hub)	$\beta_{1h,comp}$	$°$	140.3
Blade angle at leading edge (root-mean-square)	$\beta_{1rms,comp}$	$°$	141.3
Blade angle at leading edge (shroud)	$\beta_{1s,comp}$	$°$	140.7
Blade angle at trailing edge	$\beta_{2,comp}$	$°$	95
Blade number	$z_{La,comp}$	$-$	16
Blade thickness	$e_{\ comp}$	mm	0.8

B.2 Turbine's blade parameters

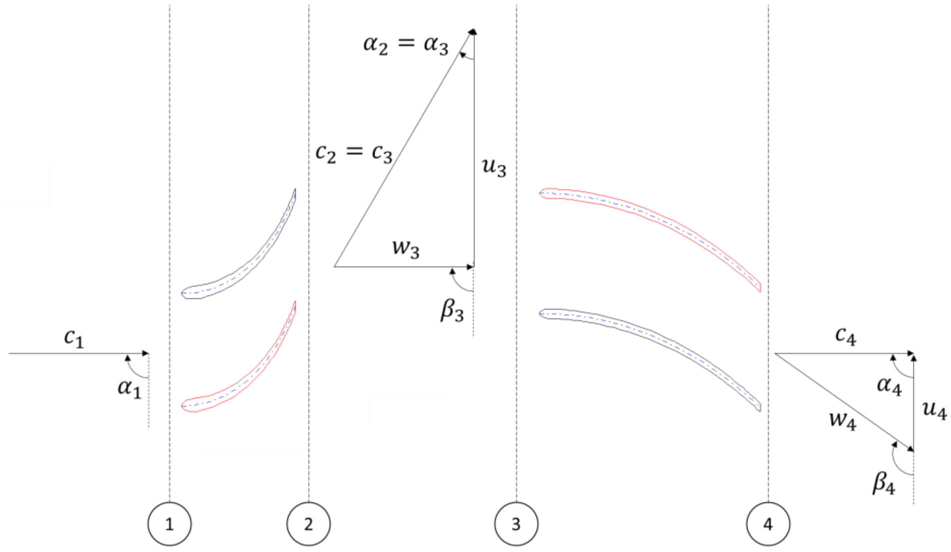

Figure 37: Velocity triangles of the turbine impeller (1→2: nozzle blades; 3→4: impeller blades)

Figure 37 illustrates the velocity triangles at the nozzle and the impeller at the design point of the turbine. The description of the parameters is given in the last part of the appendix (B.1). The design is based on a swirl-free inflow ($\alpha_1 = 90°$) and discharge ($\alpha_4 = 90°$) condition and a pure radial inlet condition at the impeller inlet ($\beta_3 = 90°$). The blades are thicker at the inlet of the nozzle and the impeller to reduce the sensitivity of the shock loss regarding the incidence angle. The information of the blade's parameters is shown below:

Parameter	Symbol	Unit	Value
Blade angle at nozzle inlet	$\alpha_{1,turb}$	°	90
Blade angle at nozzle outlet	$\alpha_{2,turb}$	°	20
Blade angle at impeller inlet	$\beta_{3,turb}$	°	90
Blade angle at impeller outlet	$\beta_{4,turb}$	°	133.9
Blade number of nozzle	$z_{Le,turb}$	–	22
Blade number of impeller	$z_{La,turb}$	–	11
Blade thickness at nozzle inlet	$e_{1,turb}$	mm	4
Blade thickness at nozzle outlet	$e_{2,turb}$	mm	0.8
Blade thickness at impeller inlet	$e_{3,turb}$	mm	3.8
Blade thickness at impeller outlet	$e_{4,turb}$	mm	0.8

B.3 Safety bearing's parameters

Parameter	Symbol	Unit	Value
Bore diameter	d	mm	60
Outside diameter	D	mm	85

Parameter	Symbol	Unit	Value
Width	B	mm	13

B.4 Labyrinth seal's design parameters

Seal position	Compressor eye	Compressor shaft	Turbine shaft	Turbine eye
Min. rotor diameter d_{min} [mm]	54	60	60	54
Max. rotor diameter d_{max} [mm]	124	124	162	162
Axial length L [mm]	20	35	35	20
Inlet pressure p_{in} [bar]	154.7	156.5	157.6	157.1
Inlet temperature T_{in} [°C]	67.9	68.4	276.6	276.5
Pressure ratio $\pi = p_{out}/p_{in}$ [bar]	0.74	0.81	0.8	0.81
Rotational speed of rotor N [rpm]	23139	23139	23139	23139
Mass flow rate at compressor inlet $\dot{m}$ [kg/s]	29.75	29.75	29.75	29.75
Leakage flow rate $\dot{m}_{lk}$ [kg/s]	1	0.74	0.22	0.28
Teeth number n [−]	3	5	5	3
Theoretical pitch l [mm]	6.67	7	7	6.67
Axial position of the seal teeth k [mm]	3.33	3.5	3.5	3.33
Seal teeth height B [mm]	1.67	1.75	1.75	1.67
Thickness of teeth peak t [mm]	0.3	0.3	0.3	0.3
Radial clearance height m [mm]	0.3	0.3	0.3	0.3
Step height H [mm]	1.5	1.5	1.5	1.5

B.5 Data sheet and performance maps of alternator "mW 17/25-4-s2r5"

Parameter	Symbol	Unit	Value
Nominal rotational speed	N	rpm	27000
Maximum rotational speed	N_{max}	rpm	29000
Frequency	f	Hz	900
Nominal power[10] (S1)	P	kW	210
Stator outer diameter	D_1	mm	170
Stator inner diameter	D_2	mm	110

[10] The nominal power is the power under a long-lived operation. The peak power is considerably higher, according to [24].

Parameter	Symbol	Unit	Value
Maximum bore diameter of the rotor	$d_{3,min}$	mm	77
Minimum bore diameter of the rotor	$d_{3,max}$	mm	72.5
Winding head length	W_1	mm	48
Winding head length	W_2	mm	34
Ring length	h	mm	8
Stack length	LFe	mm	250
Stack length	lFe	mm	250
Rotor material	–	–	Cu

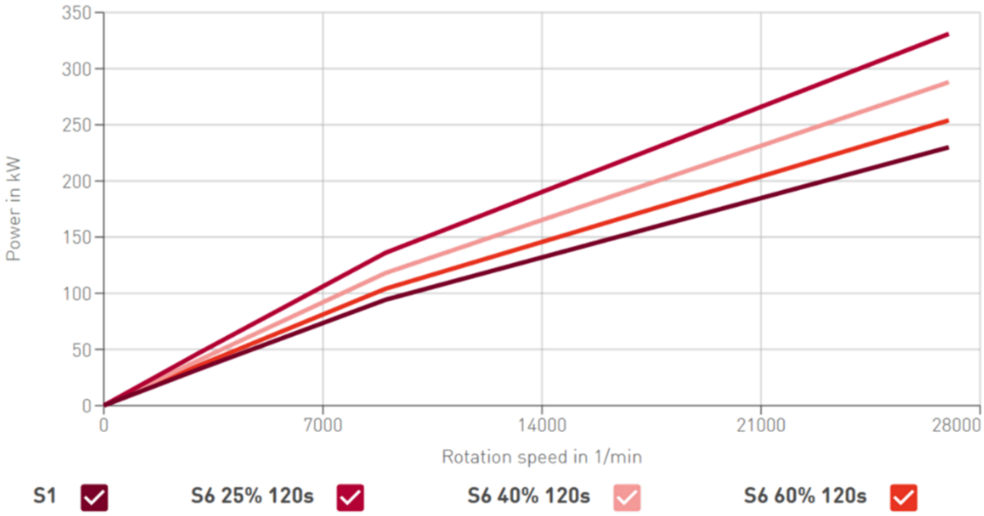

Figure 38: Power characteristics of the alternator considering S1 and S6 (extracted from the "Motor Scout")

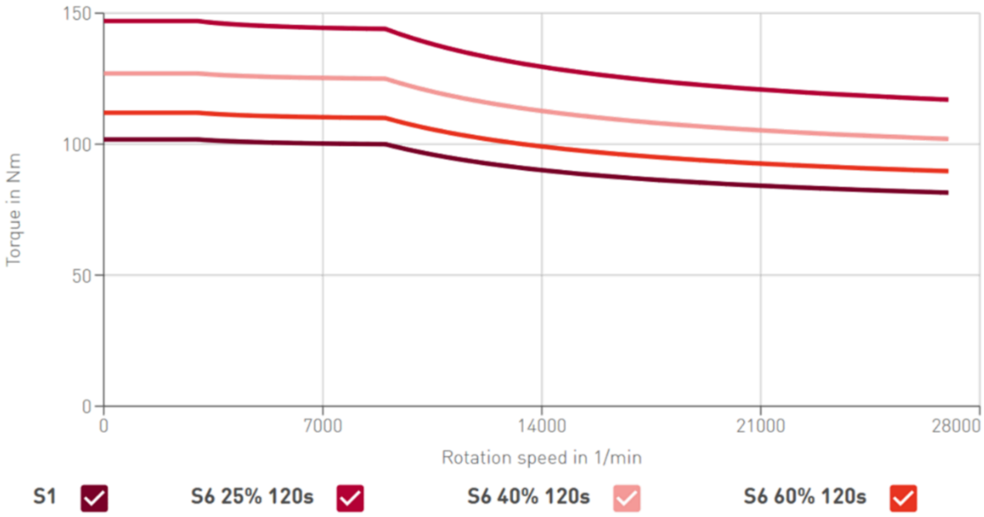

Figure 39: Torque characteristics of the alternator considering S1 and S6 (extracted from the "Motor Scout")